Spectrochimica Acta Part A: Molecular and Biomolecular Spectroscopy 241 (2020) 118667

Contents lists available at ScienceDirect

Spectrochimica Acta Part A: Molecular and Biomolecular Spectroscopy

journal homepage: www.elsevier.com/locate/saa

Synthesis of novel xanthene based analogues: Their optical properties, jack bean urease inhibition and molecular modelling studies

Balasaheb D. Vanjare [a], Prasad G. Mahajan [a], Nilam C. Dige [b], Hussain Raza [b], Mubashir Hassan [c], Sung-Yum Seo [b], Ki Hwan Lee [a,*]

[a] Department of Chemistry, Kongju National University, Gongju, Chungnam 32588, Republic of Korea
[b] Department of Biological Sciences, Kongju National University, Gongju, Chungnam 32588, Republic of Korea
[c] Institute of Molecular Biology and Biotechnology, The University of Lahore, 54590, Pakistan

ARTICLE INFO

Article history:
Received 4 April 2020
Received in revised form 17 June 2020
Accepted 27 June 2020
Available online 2 July 2020

Keywords:
Rhodamine derivatives
Photophysical properties
Urease inhibition
Radical scavenging activity
Molecular modelling

ABSTRACT

In this work, a series of the rhodamine 6G based derivatives **5a**-**5g**, were synthesized. The structural framework of the synthesized compounds was established by using ^{1}H NMR, ^{13}C NMR, FT-IR, and LC-MS analytical methods. The spectroscopic properties of the target compounds were determined by using absorption and fluorescence study in four different solvents. Furthermore, the synthesized derivatives were assessed for in-vitro screening against jack bean urease inhibition and *in-silico* molecular docking study. The result reveals that all the compounds exhibit good urease inhibitory activity against this enzyme but among the series, the compound **5a** & **5c** with an IC_{50} values of 0.1108 ± 0.0038 μM and 0.1136 ± 0.0295 μM shows to be most auspicious inhibitory activity compared to a standard drug (Thiourea) having IC_{50} value 4.7201 ± 0.0546 μM. Subsequently, the molecular docking experiment was analysed to distinguish the enzyme-inhibitor binding interaction.

1. Introduction

Nowadays, most of the scientist are engrossed in modifying or synthesizing an organic heterocyclic compound which has importance in various field such as, pharmaceutical, biotechnology and fluorescence spectroscopy [1–4]. Rhodamine and its accompanying products are a family of fluorone dye, which are one of the highly crucial heterocyclic compounds and widely used in many scientific fields [5–8]. Xanthene is one of the crucial heterocyclic scaffolds that appears in the rhodamine or its derivatives making them more active. Therefore, it has been noticed, xanthene and its derivatives have gained more admiration because of their bioactive nature [9,10]. For instance, a significant amount of xanthene core holding framework has been introduced in many therapeutically important drugs (Scheme 1) candidate containing anti-inflammatory activities, antibacterial activities, photodynamic therapy, antiviral effects, antifungal activities, and enzyme inhibition. Also, there are several reports accessible on natural products which comprise a xanthene structural frame [9,11,12].

Apart from biological applications, xanthene core containing compounds demonstrates substantial spectroscopic assets such as stokes shift, quantum yield, high molar extinction coefficient, absorption and fluorescence emission, fluorescence lifetime etc. [13–15]. Moreover, to qualify the criteria of the delicate fluorescence, the compound/dye must exhibit the finest fluorescence response when exposed in the visible scale. As per the literature survey, it has been observed that the framework containing a conjugated π-system and presence of electron-donating/withdrawing substituents in the relevant functionality, exhibit decent fluorogenic response [16]. Thus, we have integrated a rhodamine-based derivative since it comprises the xanthene structure as well as the conjugated system. In practice, rhodamine and its derivatives are rated as a versatile dye and which have been broadly utilized because of the excellent spectroscopic outcomes. Moreover, these compounds exit in two forms, one is spirocyclic close ring form (non-fluorescent) and the other is spirocyclic open ring form (fluorescent) [17]. Currently, compounds dealing with excellent spectroscopic assets have gained more consideration in the field of chemosensor, optoelectronics, cell imaging study and organic light-emitting diode (OLED) [18–20]. In this work, our major objectives were to synthesize of the novel compounds, with good yield, that are easy to replicate and target compounds that could be biologically active in contrast to different activities.

Enzyme inhibition is a standout among the highly fortunate and obligatory zones in the pharmaceutical field [21–23]. The organic chemist and pharmacist are inclined to contribute to the development of incipient medicines in the areas of biotechnology and pharmacology, due to which many valuable medicines are discovered to remedy numerous diseases [24–26]. In enzyme inhibition mechanism, the certain inhibitor binds with enzyme and blocks its activity. By blocking the action of an enzyme, it can correct the metabolic imbalance. There are

* Corresponding author.
E-mail address: khlee@kongju.ac.kr (K.H. Lee).

https://doi.org/10.1016/j.saa.2020.118667
1386-1425/

many drugs which act as an enzyme inhibitor; thus, many organic chemists are concentrating on the synthesis of the bioactive compounds [27–31].

In 1926, the scientist James Summer scrutinized that urease is a protein from its crystalline nature, that can function as an enzyme. After 70 years, the precise structure of the urease was first explained by Karplus in 1995 as Urease (E.C 3.5.1.5) which belongs to a supergroup of amidohydrolases and phosphodiesterase [32–35]. Furthermore, the first organic compound synthesized in the laboratory was urea and the first enzyme crystallized in history was urease [36–39]. It was isolated from Jack bean (JB) plant and recognized as metalloenzyme as it possesses an active site of two Nickel (II) atoms, which are involved in the hydrolysis of urea to produce volatile ammonia and carbamate. Variety of urease has expansively originated in nature among organisms, plants, microbes, green growth, and invertebrates [40–44]. Bacteria produced from urease have an adverse effect on human health. *Helicobacter pylori* is a bacteria produced from the urease which can cause infections of the urinary tract and gastrointestinal [45–47]. Some other diseases related with urease are hepatic coma, urinary catheter encrustation, hepatic encephalopathy, pyelonephritis, urolithiasis, etc. Urease inhibitors have a crucial function in the inhibition of harmful consequence caused by urease enzyme and significantly help to recuperate human health [48–50a].

Herein, we have constructed and synthesized numerous rhodamine 6G centered derivatives by the reaction of the rhodamine 6G and different hydrazide compounds in basic media. The structural interpretation of the synthesized compounds was confirmed by using different analytical techniques, for instance, LCMS, ^{1}H NMR, ^{13}C NMR & FT-IR spectroscopy skills. The spectroscopic properties of the synthesized target compounds have been evaluated in distinct solvents including non-polar, polar-aprotic, and polar protic solvents. Moreover, from the biomedical applications point of view, the synthesized target compounds were screened against urease inhibitory activity. From the in-vitro study, we observed that distinct substituent appears in nucleophile and significantly influences the urease inhibitory activity. Additionally, the bioactivity outcomes were endorsed by the free radical scavenging survey and the molecular modelling studies.

2. Materials and methods

2.1. Chemistry

All the reagents were procured from Sigma Aldrich and solvents required in synthesis, purification technique and for photophysical study were purchased from Samchun chemicals (Daejeon, South Korea), which were used without purification. ^{1}H NMR and ^{13}C NMR for the synthesized target compounds were undertaken at 400 MHz spectrophotometers in DMSO-d_6 solvent, by using a Bruker Avance (Germany). The chemical shift and coupling constant values mentioned in ppm and Hz, respectively. The mass analysis (LC-MS) was recorded on 2795/ZQ2000 (waters) spectrometer. The FT-IR spectra were recorded on Fourier IR spectrophotometer (Perkin Elmer, USA). The reaction progress was tracked by a thin layer chromatography (TLC) method. The melting points of the compounds (**5a**-**5g**) were determined by using Fisher Scientific (USA) melting point instrument and are uncorrected. The UV–Visible absorption and fluorescence emission spectra of the target compounds (**5a**-**5g**) were computed on a Shimadzu Spectrophotometer and FS-2 fluorescence spectrophotometer (Scinco, Korea). The UV–Visible absorption and emission spectra of the targets compound were measured in various solvents like chloroform ($CHCl_3$), acetonitrile (ACN), dimethyl formamide (DMF) and methanol (MeOH) at 100 μM (1×10^{-4} mol/L). Path length of the cells used for absorption and emission studied was 1 cm. The decay curves were obtained using a Time Correlated single photon counting (TCSPC) spectrophotometer (HORIBAiHR320) employing a nanosecond diode laser with time correlation of 0.0548 ns per channel and operated at its respective wavelength (530–560 nm). The fluorescence quantum yield of the target compounds (**5a**-**5g**) in different solvents were determined by using Eq. (1).

$$\Phi_{sample} = \Phi_{ref} \times \frac{OD_{ref} \times A_{sample} \times \eta^2{}_{sample}}{OD_{sample} \times A_{ref} \times \eta^2{}_{ref}} \quad (1)$$

where, A represents the area under the fluorescence spectra and OD is optical density of the compound at the excitation wavelength, η is the refractive index of the solvent used. Quinine sulphate in 0.1 M sulphuric acid was taken as the reference (Φ_f) = 0.546 [2].

2.1.1. General method for the synthesis of compounds (2a-2g), (3a-3g) and (5a-5g)

2.1.1.1. General procedure for the Synthesis of (2/3/4) un/substituted ethyl benzoate (2a-2g). As presented in Scheme 2, the unsubstituted/substituted aromatic acid compound (**1a**-**1g**, 1 mmol) were dissolved in ethanol (15 mL) and stirred for 10 min. Concentrated H_2SO_4 was added to it and followed by refluxing for 5–6 h. The formation of the product was checked by using TLC in hexane/Ethyl acetate (4:6) [50a]. After completion of the reaction, the reaction mass was gradually cooled to ambient temperature and concentrated by rotary evaporator. Water was added to the residue and extracted by using ethyl acetate. Further, ethyl acetate part (organic layer) was washed by a saturated solution of sodium bicarbonate (to remove the excess of acid) and followed by water and brine washing. The ethyl acetate layer was dried over anhydrous magnesium sulphate, filtered, and distilled to afford a (**2a**-**2g**) with 70–80% yield and used for the next step.

2.1.1.2. General procedure for the synthesis of (2/3/4) un/substituted-benzhydrazides (3a-3g). As displayed in Scheme 2, the un/substituted ester derivative (**2a**-**2g**, 1.0 mmol), hydrazine hydrate (1.2 mmol) were taken in ethyl alcohol (10 mL) and the reaction mixture was heated to reflux temperature and maintained until the reaction was completed (Checked by TLC) [50a]. After achievement of the reaction, the reaction was progressively cooled to room temperature. Slowly, solid precipitated out in the reaction mass, was filtered, washed with cold ethanol, and dried to afford a product (2/3/4) un/substituted-Benz hydrazides with 80–87% yield (**3a**-**3g**).

2.1.1.3. General procedure for the synthesis of N-(3′,6′-bis(ethyl amino)-2′,7′-dimethyl-3-oxospiro[isoindoline-1,9′-xanthene]-2-yl) (2/3/4-un/substituted-benzamides) compounds (5a-5g). As shown in Scheme 2, rhodamine 6G (1.0 mmol) and compound (**3a**-**3g**) (1.0 mmol) were taken in DMF (8 mL) and cooled to 0–5 °C. Potassium tert-butoxide was added slowly and the reaction was stirred at 0–5 °C for 1 h then the temperature was gradually augmented to 25–30 °C and stirred until the reaction gets completed (6–7 h/monitored by TLC) [50b]. The reaction mixture was quenched by gradual addition of the ice-cold water, the solid gets suspended in the reaction mass which was finally filtered and dried. The impure solid was purified by column chromatography, using dichloromethane/methanol (9.5:0.5) as an eluent to afford a pink coloured target compound with 80–86% yield (**5a**-**5g**).

2.1.1.3.1. N-(3′,6′-bis(ethyl amino)-2′,7′-dimethyl-3-oxospiro [isoindoline-1,9′-xanthene]-2-yl)benzamide (5a). Pink solid; Melting point: >260 °C; Yield 80%; Fig. ES1: ^{1}H NMR (400 MHz, DMSO-d_6) δ 10.09 (s, 1H, -NH), 7.86 (d, J = 6.8 Hz, 1H, Ar—H), 7.66–7.32 (m, 7H, Ar—H), 7.02 (d, J = 6.9 Hz, 1H, Ar—H), 6.32 (s, 2H, Ar—H), 6.20 (s, 2H, Ar—H), 4.98 (s, 2H, [-**NH**-CH_2-CH_3]$_2$), 3.21–3.01 (m, 4H, [-**CH_2**-CH_3]$_2$), 1.86 (s, 6H, Ar-**CH_3**), 1.19 (t, J = 7.1 Hz, 6H, [-CH_2-**CH_3**]$_2$). Fig. ES2: ^{13}C NMR (101 MHz, DMSO-d_6) δ 170.64, 166.11, 162.46, 152.33, 147.82, 132.82, 128.85, 122.67, 117.87, 104.87, 96.13, 55.49, 37.93, 17.66, 14.83. Fig. ES3: IR (KBr, cm^{-1}): 3401.41 (-**NH**-COAr), 3355.10 (Ar-**NH**-CH_2-CH_3), 3239.17, 3022.15 (aromatic alkene

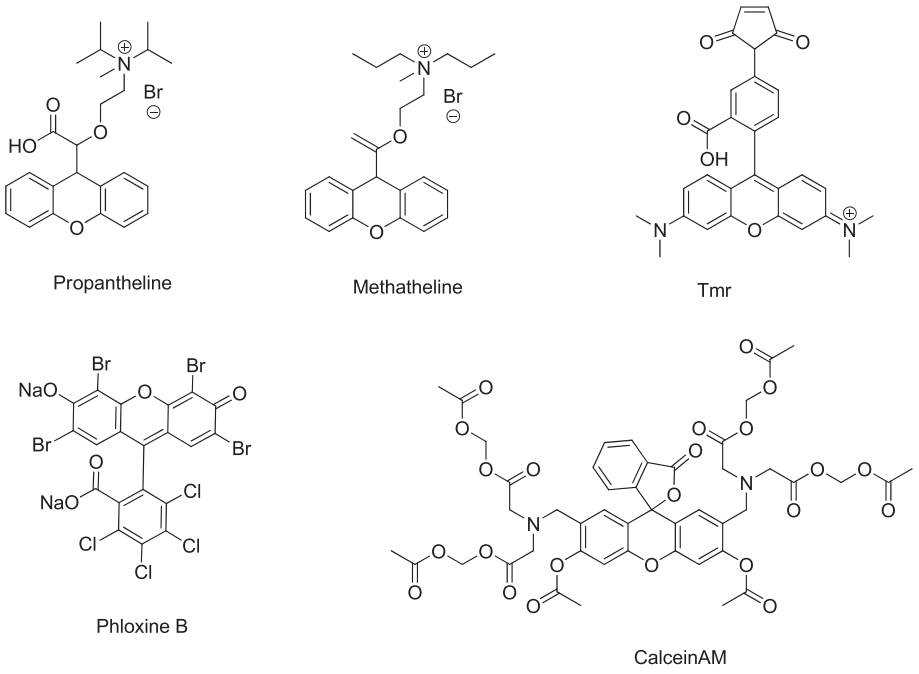

Scheme 1. Biologically crucial structure of xanthene derivatives.

stretching -C=**C-H**), 2969.87 (aliphatic -NH-**C-H$_2$-**CH$_3$), 2868.22 (aliphatic -NH-CH$_2$-**C-H$_3$**), 1680.79 (Secondary amide -NH-**CO**-Ar), 1202.68 (aromatic amine C—N); Fig. ES4: LC-MS: 533.6 *m/z*.

2.1.1.3.2. N-(3′,6′-bis (ethyl amino)-2′,7′-dimethyl-3-oxospiro [isoindoline-1,9′-xanthene]-2-yl)-2-hydroxybenzamide (5b). Pink solid; Melting point: 147 °C; Yield 82%. Fig. ES5: ^{1}H NMR (400 MHz, DMSO) δ 11.39 (s, 1H, -OH), 9.93 (s, 1H, -NH), 7.90–7.77 (m, 1H, Ar—H), 7.68 (dd, J = 8.1, 1.6 Hz, 1H, Ar—H), 7.62–7.52 (m, 2H, Ar—H), 7.40–7.33 (m, 1H, Ar—H), 7.01 (dd, J = 7.9, 4.2 Hz, 1H, Ar—H), 6.87–6.81 (m, 2H, Ar—H), 6.36 (m, 2H, Ar—H), 6.20 (m, 2H, Ar—H), 5.03 (s, 2H, [-**NH**-CH$_2$-CH$_3$]$_2$), 3.16–3.02 (m, 4H, [-NH-**CH$_2$**-CH$_3$]$_2$), 1.88 (s, 6H, Ar-**CH$_3$**), 1.19 (t, J = 7.1 Hz, 6H, [-NH-CH$_2$-**CH$_3$**]$_2$). Fig. ES6: ^{13}C NMR (101 MHz, DMSO) δ 163.85, 160.76, 152.02, 148.04, 129.98, 128.84, 117.86, 117.04, 116.13, 105.14, 104.01, 95.57, 37.94, 17.61, 14.53. Fig. ES7: IR

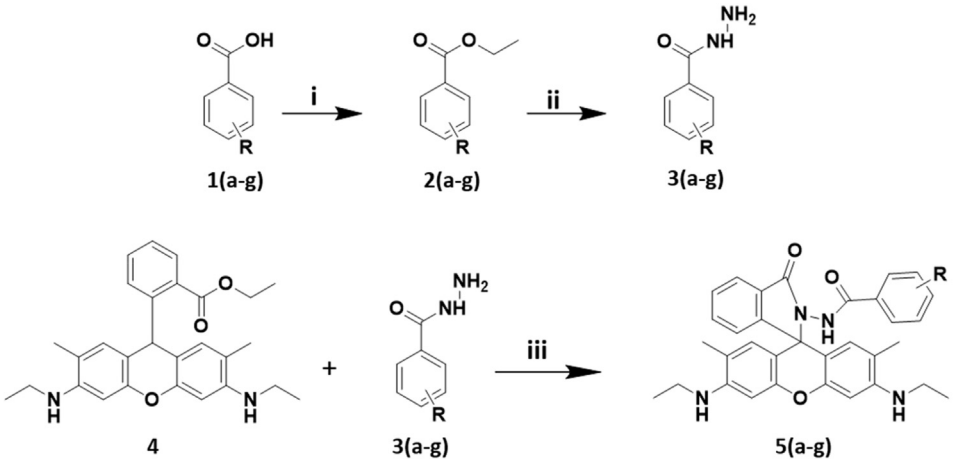

Different Substituted Aromatic Acid Used:

1a	1b	1c	1d	1e	1f	1g
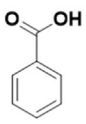	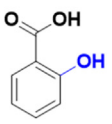	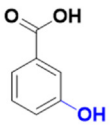	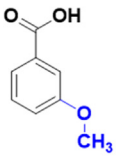	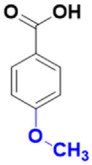		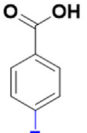

Scheme 2. Synthesis route, reagents, and conditions: i) ethanol, conc. H_2SO_4 ii) hydrazine hydrate, ethanol, reflux. iii) Potassium tert-butoxide (K-tOBu), DMF, RT.

(KBr, cm^{-1}): 3324.86 (Ar-**NH**-CH_2-CH_3), 2929.31 (aliphatic -NH-**C-H_2-**CH_3), 2851.22 (aliphatic -NH-CH_2-**C-H_3**), 1623.69 (Secondary amide -NH-**CO**-Ar), 1513.04 (-C=C-), 1218.28 (aromatic amine C—N); Fig. ES8: LC-MS: 549 *m/z*.

2.1.1.3.3. N-(3′,6′-bis(ethyl amino)-2′,7′-dimethyl-3-oxospiro [isoindoline-1,9′-xanthene]-2-yl)-3-hydroxybenzamide (5c). Pink solid; Melting point: 120 °C; Yield 80%. Fig. ES9: ^{1}H NMR (400 MHz, DMSO) δ 10.04 (s, 1H, -NH), 7.96–7.16 (m, 5H, Ar—H), 7.15–6.96 (m, 3H, Ar—H), 6.31 (s, 2H, Ar—H), 6.19 (s, 2H, Ar—H), 4.98 (s, 2H, [-**NH**-CH_2-CH_3]$_2$), 3.16–3.05 (m, 4H, [-NH-**CH_2**-CH_3]$_2$), 1.86 (s, 6H, Ar-**CH_3**), 1.19 (t, J = 7.1 Hz, 6H, [-NH–CH_2-**CH_3**]$_2$). Fig. ES10: ^{13}C NMR (101 MHz, $CdCl_3$) δ 152.38, 147.82, 129.44, 128.83, 123.61, 117.32, 104.62, 95.83, 61.25, 50.79, 38.27, 30.74, 16.59, 14.47; Fig. ES11: IR (KBr, cm^{-1}): 3323.83 (secondary amine Ar-**NH**-CH_2CH_3), 2929.26 (aliphatic -NH-**C-H_2-**CH_3), 2851.29 (aliphatic -NH-CH_2-**C-H_3**), 1705.24 (carbonyl), 1621.96 (Secondary amide -NH-**CO**-Ar), 1217.82 (aromatic amine C—N), 903.67 (monosubstituted); Fig. ES12: LC-MS: 549.3 *m/z*.

2.1.1.3.4. N-(3′,6′-bis(ethyl amino)-2′,7′-dimethyl-3-oxospiro [isoindoline-1,9′-xanthene]-2-yl)-3-methoxybenzamide (5d). Pink solid; Melting point: 252 °C; Yield 83%, Fig. ES13: ^{1}H NMR (400 MHz, DMSO) δ 9.98 (s, 1H, -NH), 7.84 (d, J = 7.2 Hz, 1H, Ar—H), 7.62–7.51 (m, 2H, Ar—H), 7.18–7.12 (m, 1H, Ar—H), 7.06–6.91 (m, 3H, Ar—H), 6.86 (dd, J = 8.1, 2.5 Hz, 1H, Ar—H), 6.32 (s, 2H, Ar—H), 4.97 (s, 2H, Ar—H), 3.82 (s, 3H, -OCH_3), 4.97 (s, 2H, [-**NH**-CH_2-CH_3]$_2$), 3.20–3.01 (m, 4H, [-NH-**CH_2**-CH_3]$_2$), 1.86 (s, 6H, AR-CH_3), 1.19 (t, J = 7.1 Hz, 6H, [-NH-**CH_2**-CH_3]$_2$). Fig. ES14: ^{13}C NMR (101 MHz, CdCl3) δ 152.44, 147.76, 133.96, 133.38, 129.41, 129.11, 129.06, 128.51, 123.56, 119.39, 118.26, 115.37, 96.35, 50.68, 38.40, 30.92, 29.76, 16.72, 14.69; Fig. ES15: IR (KBr, cm^{-1}): 3400.03 (aliphatic -NH-CH_2-**C-H_3**), 3246.00, 3022.15 (aromatic alkene stretching -C=**C-H**), 2970.22 (aliphatic -NH-**C-H_2-**CH3), 2870.26 (aliphatic -NH-CH_2-**C-H_3**), 1680.32 (Secondary amide -NH-**CO**-Ar), 1272.95 (aromatic amine C—N), 967.31 (monosubstituted); Fig. ES16: LC-MS: 563.4 *m/z*.

2.1.1.3.5. N-(3′,6′-bis (ethyl amino)-2′,7′-dimethyl-3-oxospiro [isoindoline-1,9′-xanthene]-2-yl)-4-methoxybenzamide (5e). Pink solid; Melting point: 170 °C; Yield 87%, Fig. ES17: ^{1}H NMR (400 MHz, DMSO) δ 10.01 (s, 1H, -NH), 8.00–7.73 (m, 1H, Ar—H), 7.62–7.45 (m, 4H, Ar—H), 7.29–7.11 (m, 1H, Ar—H), 7.02 (dd, J = 26.0, 7.4 Hz, 1H, Ar—H), 6.92–6.91 (s, 1H, Ar—H), 6.30 (s, 2H, Ar—H), 6.21 (s, 2H, Ar—H), 4.97 (s, 2H, [-**NH**-CH_2-CH_3]$_2$), 3.76 (s, 3H, -OCH_3), 3.14–3.07 (m, 4H, [-NH-**CH_2**-CH_3]$_2$), 1.86 (s, 6H, Ar-CH_3), 1.19 (t, J = 7.1 Hz, 6H, [-NH-CH_2-**CH_3**]$_2$). Fig. ES18: ^{13}C NMR (101 MHz, DMSO) δ 165.16, 164.16, 162.64, 152.26, 148.27, 130.26, 124.86, 124.58, 123.18, 117.55, 113.91, 104.58, 95.53, 66.16, 55.99, 37.67, 17.91, 14.53. Fig.ES19: IR (KBr, cm^{-1}): 3402.92 (-**NH**-COAr), 3241.52 (Ar-**NH**-CH_2-CH_3), 3022.11 (aromatic alkene stretching -C=**C-H**), 2970.10 (aliphatic -NH-**C-H_2-**CH3), 2870.05 (aliphatic -NH-CH_2-**C-H_3**), 1682.71 (Secondary amide -NH-**CO**-Ar), 1273.49 (aromatic amine C—N), 967.30; Fig. ES20: LC-MS: 563.6 *m/z*.

2.1.1.3.6. N-(3′,6′-bis(ethyl amino)-2′,7′-dimethyl-3-oxospiro [isoindoline-1,9′-xanthene]-2-yl)-2-fluorobenzamide (5f). Pink solid; Melting point: >260 °C; Yield 80% Fig. ES21: ^{1}H NMR (400 MHz, DMSO) δ 10.01 (s, 1H, -NH), 7.86 (dd, J = 6.5, 1.5 Hz, 1H, Ar—H), 7.62–7.55 (m, 2H, Ar—H), 7.52–7.41 (m, 1H, Ar—H), 7.37–7.13 (m, 3H, Ar—H), 7.04 (d, J = 6.7 Hz, 1H, Ar—H), 6.27 (s, 2H, Ar—H), 6.23 (s, 2H, Ar—H), 4.99 (s, 2H, [-**NH**-CH_2-CH_3]$_2$), 3.18–3.04 (m, 4H, [-NH-**CH_2**-CH_3]$_2$), 1.84 (s, 6H, Ar-CH_3), 1.19 (t, J = 7.1 Hz, 6H, [-NH-CH_2-**CH_3**]$_2$); Fig. ES22: ^{13}C NMR (101 MHz, DMSO) δ 163.89, 162.99, 161.53, 155.90, 152.19, 152.01, 148.03, 129.46, 128.95, 124.49, 123.10, 117.76, 104.52, 95.82, 66.16, 55.38, 37.94, 17.62, 14.68. Fig. ES23: IR (KBr, cm^{-1}): 3403.29 (-**NH**-COAr), 3250.36 (Ar-**NH**-CH_2-CH_3), 3022.16 (aromatic alkene stretching -C=**C-H**), 2969.98 (aliphatic -NH-**C-H_2-**CH_3), 2868.97 (aliphatic -NH-CH_2-**C-H_3**), 1682.66 (Secondary amide -NH-**CO**-Ar), 1273.52 (aromatic amine C—N), 967.34; Fig. ES24: LC-MS: 551.6 *m/z*.

2.1.1.3.7. N-(3′,6′-bis(ethyl amino)-2′,7′-dimethyl-3-oxospiro [isoindoline-1,9′-xanthene]-2-yl)-4-fluorobenzamide (5g). Pink solid; Melting point: >260 °C; Yield 85%, Fig. ES25: ^{1}H NMR (400 MHz, DMSO) δ 10.01 (s, 1H, -NH), 7.86 (dd, J = 6.4, 1.5 Hz, 1H, Ar—H), 7.58 (m, 2H, Ar—H), 7.47 (m, 1H, Ar—H), 7.31–7.13 (m, 3H, Ar—H), 7.04 (dd, J = 6.5, 1.3 Hz, 1H, Ar—H), 6.27 (s, 2H, Ar—H), 6.23 (s, 2H, Ar—H), 5.00 (s, 2H, [-**NH**-CH_2-CH_3]$_2$), 3.15–3.03 (m, 4H, [-NH-**CH_2**-CH_3]$_2$), 1.84 (s, 6H, Ar-CH_3), 1.19 (t, J = 7.1 Hz, 6H, [-NH-CH_2-**CH_3**]$_2$). Fig. ES26: ^{13}C NMR (101 MHz, CdCl3) δ 152.28, 151.75, 147.74, 133.81, 132.16, 128.87, 128.46, 123.55, 117.88, 116.08, 115.84, 104.54, 96.44, 50.67, 38.41, 30.91, 16.72, 14.68; Fig. ES27: IR (KBr, cm^{-1}): 3401.67 (-**NH**-COAr), 3240.23 (Ar-**NH**-CH_2-CH3), 3022.18 (aromatic alkene stretching -C=**C-H**), 2970.22 (aliphatic -NH-**C-H_2-**CH_3), 2870.72 (aliphatic -NH-CH_2-**C-H_3**), 1683.20 (Secondary amide -NH-**CO**-Ar), 1274.04 (aromatic amine C—N), 967.31; Fig. ES28: LC-MS: 551.6 *m/z*.

2.2. Biological evaluation

2.2.1. In-vitro urease inhibition activity

For the synthesized molecules, the in-vitro studies were performed by evaluating them against the jack bean urease enzyme. The enzyme (Jack bean urease) activity was determined by evaluating the absorbance and the amount of ammonia generated using the already reported indophenol technique [51–54]. The reaction mixture contained enzyme (20 μL) (Jack bean urease, 5 U/mL) and 20 μL respective compounds (**5a**-**5g**) in 50 μL potassium phosphate buffer (100 mM urea, 10 mM K_2HPO_4, 1 mM EDTA and 10 mM LiCl, pH 8.2), were incubated at 37 °C in 96-well plate for 30 min. Briefly, each well was supplemented with 50 μL each of phenol reagents (1%, w/v phenol and 0.005%, *w/v* sodium nitroprusside) and 50 μL of alkali reagent (0.5%, w/v NaOH and 0.1% Sodium hypochlorite (NaOCl)). Absorbance was measured after 10 min by using a microplate reader (OPTI Max, Tunable USA) at 625 nm. All the measurements were conducted in triplicate. The urease inhibition activities were calculated by using the Eq. (2).

$$\text{Urease Inhibition Activity } (\%) = \left[OD_{control} - OD_{sample}/OD_{control}\right] \times 100 \quad (2)$$

where, $OD_{control}$ and OD_{sample} indicate the optical densities in the absence and presence of the sample, respectively. Thiourea has been used as positive control for the activity of urease.

2.2.2. Kinetic analysis

The mode of inhibition was determined by kinetic analysis study. Based on the most powerful IC_{50} values, compound **5a** was chosen. Kinetics have been achieved by varying the urea concentration in the vicinity of distinct concentrations of compound **5a** (0.00, 0.06, 0.12 and 0.24 μM). In urease kinetics study, the concentration of the urea was ranged from 100, 50, 25, 12.5, 6.25 and 3.12 mM, respectively, but the rest of the procedure was same for all kinetic study as described in urease inhibition assay protocol. Maximum initial velocities were determined from the original absorbance part, up to 10 min later the enzyme was added at the interval of each minute. The type of the inhibition on the enzyme was scrutinized by plotting a Lineweaver-Burk graph of inverse of velocities (1/V) against the inverse of substrate concentration 1/[S] mM^{-1}. In addition, the EI dissociation constant (Ki) was calculated by plotting a secondary graph of 1/V against inhibitor concentration. Urease activity was measured using the indophenol method as earlier reported by evaluating ammonia quantification. Urease activity was determined by measuring ammonia production using the indophenol method as reported previously [55–57]. The results (change in absorbance per min) were processed by using SoftMaxPro.

2.2.3. Free radical scavenging assay

Radical scavenging activity was not easily affected by altering a previously reported technique [58,59] by 2,2-diphenyl-1 picrylhydrazyl (DPPH) assay. The test solution consisted of 100 μL of DPPH (150 μM), 20 μL of increasing concentration of test compounds and the volume was adapted to 200 μL with methanol in each well. Afterward, the assay reaction mixture was incubated at ambient temperature for 30 min. Furthermore, Ascorbic acid (Vitamin C) was used as a reference inhibitor. Measurements of the assay were achieved by using a microplate reader (OPTI Max, Tunable) at 517 nm. In this study, we compared the reaction rates, and calculated the percent inhibition induced by the presence of tested inhibitors. All experiments were repeated thrice.

2.3. In-silico methodology

2.3.1. Retrieval of Jack bean urease in protein preparation wizard

The structure of the jack bean urease was gained from Protein Data Bank (PDB) (www.rcsb.org) having PDBID 4H9M in protein preparation wizard. The preferred urease protein structure has been pre-processed, improved, and minimized using Maestro interface default parameters [60].

2.3.2. Grid generation and molecular docking

The improved Jack bean urease structure was organized using the "Protein Preparation Wizard" workflow in Schrödinger Suite before molecular docking. Bond orders were assigned, and hydrogen atoms were supplemented with hydrogen atoms. The structure was then minimized with the OPLS_2005 force field to achieve a converged root mean square deviation (RMSD) of 0.30 Å. The active site of the enzyme is defined from the co-crystallized ligands from Protein Data Bank and literature data [61,62]. Furthermore, the docking experiment was performed against all synthesized ligands (**5a-5g**) sketched in 2D sketcher and target protein by using the Glide docking protocol [63]. By using Glide experiment, the anticipated binding energies (docking ratings) and conformational positions of the ligands within the active protein section were also performed. Throughout the docking simulations, both partial flexibility and full flexibility around the active site residues are performed by Glide/SP/XP and induced fit docking (IFD) approaches [64].

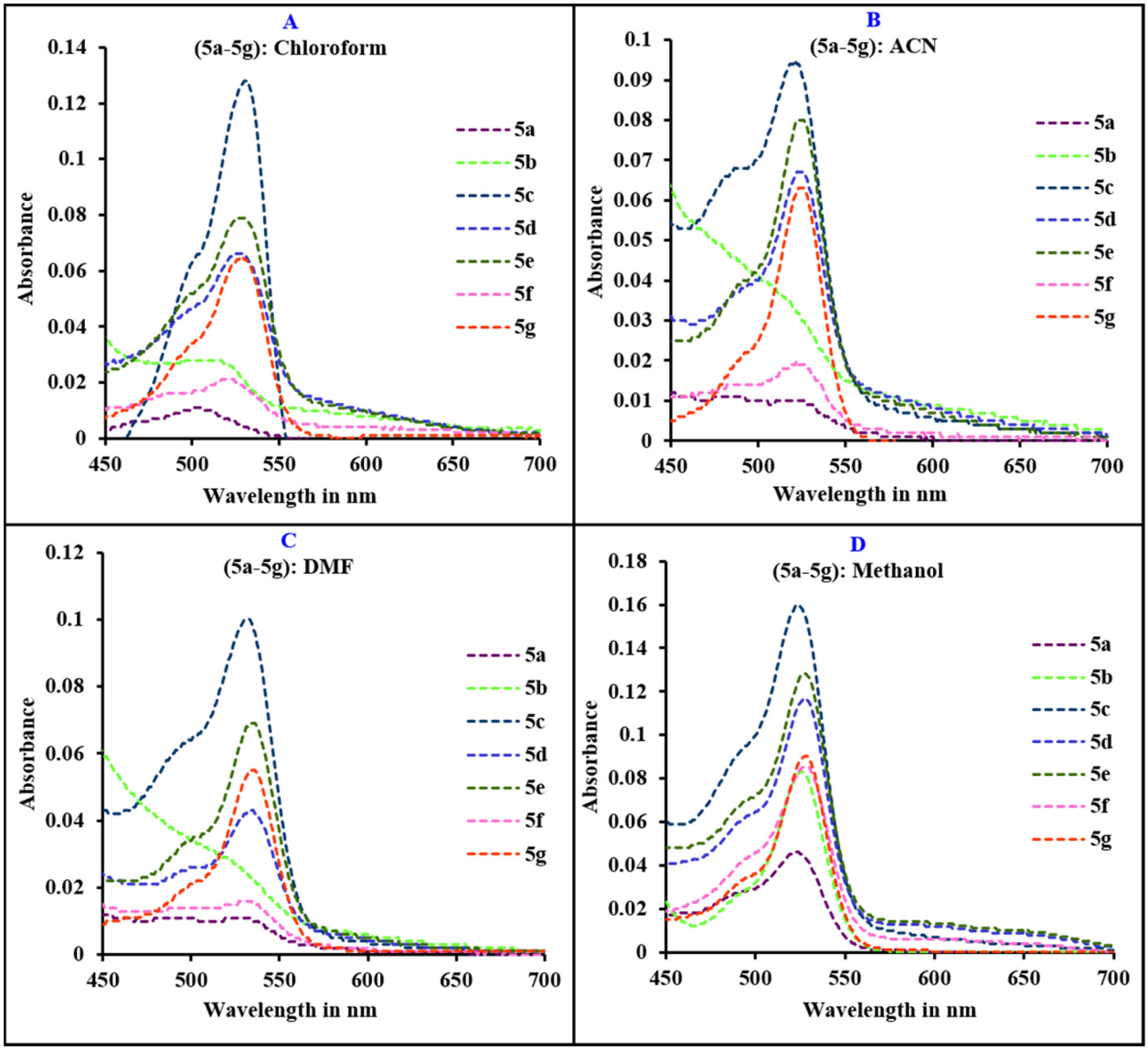

Fig. 1. UV–Vis absorption spectra of the target compounds (5a-5g) at 1×10^{-4} mol/L in different solvents such as A) chloroform B) ACN C) DMF and D) methanol.

3. Results and discussion

3.1. Chemistry

3.1.1. Synthesis

The synthetic path for rhodamine derivatives (5a-5g) is presented in Scheme 2. The various aromatic ester derivatives (**2a**-**2g**) were prepared by reacting the acid compounds (**1a**-**1g**) in ethanol, refluxed under acidic condition. Further, the un/substituted ester derivatives were reacted at reflux temperature with hydrazine hydrate in ethanol. This replacement reaction was performed to insert a hydrazide functionality (**3a**-**3g**) into the various acid derivatives, these un/substituted hydrazide derivatives were further used for the synthesis of the target compounds (**5a**-**5g**). Finally, the equivalent rhodamine 6G derivatives were synthesized by the reaction of the different un/substituted aromatic benzhydrazide (**3a**-**3g**) with rhodamine 6G in presence of anhydrous potassium tert-butoxide under nitrogen atmosphere at ambient temperature. However, the progress of the reaction was checked by TLC technique. The synthesized target compounds were purified by using column chromatography method, in which the crude solid of target compounds (**5a**-**5g**), initially adsorbed on silica (60–120 mesh), and the column was packed using 100–200 mesh size silica, in which dichloromethane (MDC) and methanol used as an eluting solvent. Afterwards, a single spot on TLC was segregated individually for all the target compounds (**5a**-**5g**). Finally, the structural clarification of the target compounds (**5a**-**5g**) was done by using FT-IR, LC-MS, ^{1}H NMR and ^{13}C NMR analytical methods.

3.1.2. Photophysical study

The absorption and emission spectra of the target compounds were assessed in variety of solvents including non-polar (chloroform), polar aprotic (ACN and DMF) and polar protic (methanol) solvents at 100 μM (1×10^{-4} M). The absorption and emission graphs were used to evaluate the spectroscopic parameters for instance absorption and emission wavelength, Stokes shift, molar extinction coefficient, fluorescence quantum yield, and fluorescence lifetime values of the respective compounds in a variety of solvents. Fig. 1A, B, C, and D relates to absorption spectra of the target compounds (**5a**-**5g**) in four distinct solvents such as chloroform, ACN, DMF, and methanol. Fig. 1A demonstrates maximum absorption band within the spectral region 500–530 nm for the compounds **5a**-**5g** in chloroform. Similarly, Fig. 1B, C and D exhibits the absorption maxima ranges from 520 to 535 nm, 530–540 nm, and 520–530 nm in ACN, DMF and methanol solvent, respectively. The bands showed in the absorption spectra were attributed to the $\pi \rightarrow \pi^{*}$

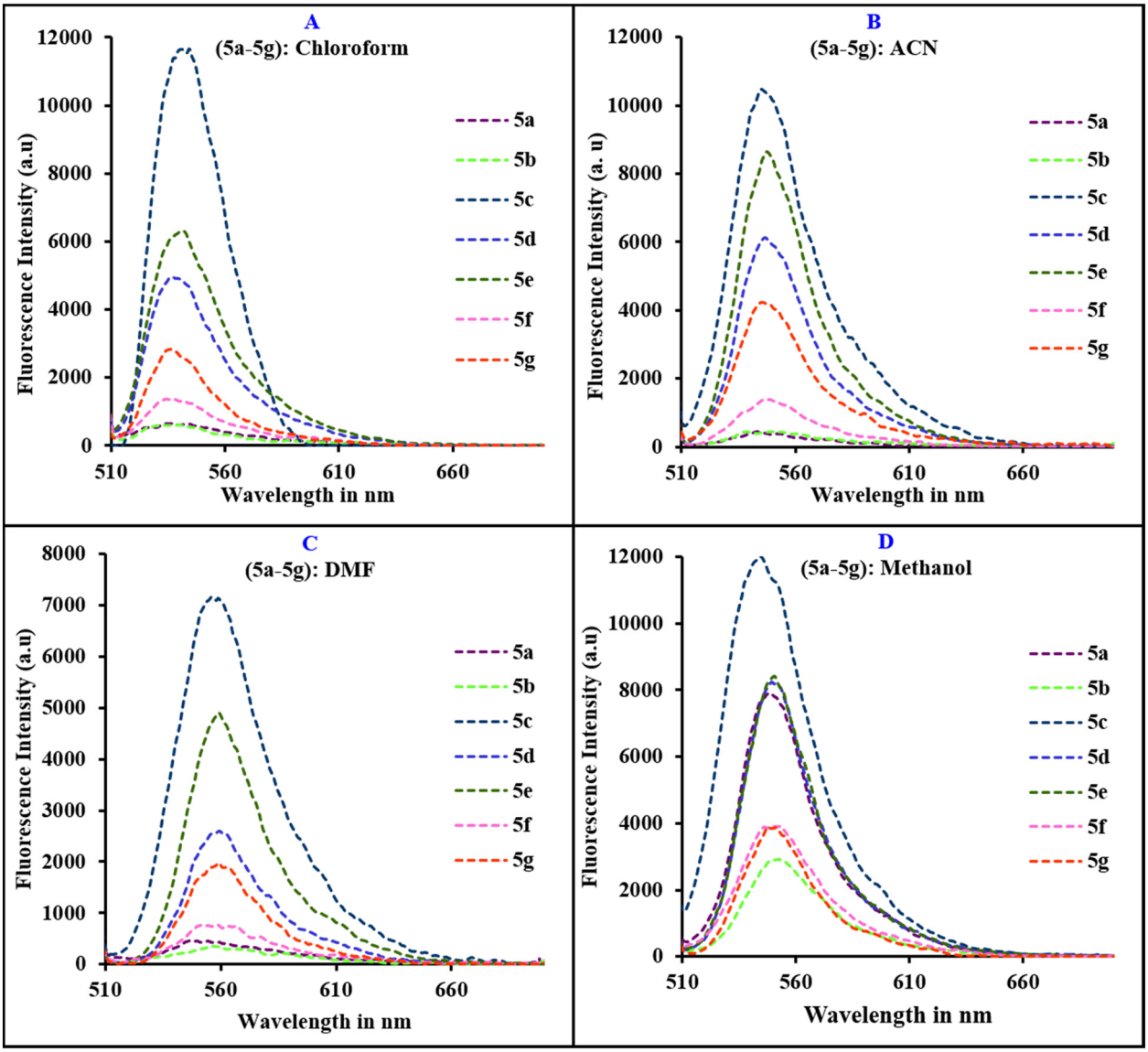

Fig. 2. Fluorescence emission spectra of compounds (5a-5g) at 1×10^{-4} mol/L in different solvents such as A) chloroform B) ACN C) DMF and D) methanol.

Table 1
Photophysical properties presented by compounds **5a**-**5g** in chloroform, ACN, DMF and methanol solvent.

Compound	λ_{abs} (nm)	λ_{em} (nm)	Stokes shift (nm)	ε (M^{-1} cm^{-1})	ϕ_f	τ (ns)
Chloroform ($CHCl_3$)						
5a	507	535	28	110	0.094	3.17
5b	523	536	13	260	0.035	3.07
5c	532	540	8	1280	0.083	3.55
5d	529	538	9	660	0.080	3.26
5e	530	543	13	790	0.099	3.27
5f	524	538	14	210	0.086	3.44
5g	530	536	6	640	0.041	3.42
Acetonitrile (ACN)						
5a	531	545	14	90	0.062	2.68
5b	522	550	28	320	0.022	2.35
5c	522	546	24	940	0.132	3.43
5d	525	547	22	670	0.095	3.27
5e	525	549	24	800	0.127	3.38
5f	526	548	22	190	0.079	3.16
5g	525	545	20	630	0.072	3.32
Dimethylformamide (DMF)						
5a	538	555	17	100	0.081	3.19
5b	537	557	20	210	0.027	2.10
5c	531	557	26	1000	0.090	3.43
5d	535	560	25	430	0.074	3.06
5e	535	560	25	690	0.087	3.26
5f	537	557	20	150	0.066	3.16
5g	535	560	25	550	0.036	3.55
Methanol (MeOH)						
5a	525	548	23	460	0.219	3.19
5b	527	552	25	820	0.040	2.05
5c	524	545	21	1600	0.091	3.13
5d	527	550	23	1170	0.084	2.59
5e	530	551	21	1270	0.078	2.65
5f	530	550	20	850	0.054	3.05
5g	529	550	21	990	0.039	3.33

λ_{abs} = Maximum absorption wavelength; λ_{em} = fluorescence emission wavelength; ε = molar extinction coefficient; ϕ_f = fluorescence quantum yield and τ = fluorescence lifetime.

transitions of the conjugated skeleton on the xanthene ring. Therefore, from the absorption spectrum can be stated that, as the polarity of the solvent enhances from non-polar to polar aprotic solvent, the absorption maxima slightly changes towards red shift. A small spectral shift was observed in chloroform, ACN and DMF solvents but in case of polar protic solvent (methanol), it switched towards blue zone. Besides, if the electron donating substituents (like —F, -OH or -OCH_3) are present at ortho position or in the absence of substituents with respect to carbonyl group, under such scenario the compounds (**5a**, **5b** and **5f**) exhibits an increased peak broadening along with reduced absorbance values. The variation of the results might be arisen because of the ortho substituted (**5b** & **5f**)/unsubstituted (**5a**) xanthene compounds, can influence to the conjugated π-electrons system causes to restriction the transition from bonding molecular orbital to the antibonding molecular orbital. This sort of behaviour has been detected in chloroform, ACN and DMF solvents but not in case of methanol. In details, rhodamine and its derivative consist of a highly strained five membered spirocyclic ring. In the presence of the polar protic solvent such as methanol, xanthene associated amino group gets protonated causing delocalization of the π electrons and results into the opening of the spirocyclic ring [65]. As a result, the absorbance intensity of the synthesized target compounds rises in polar protic solvent but the same is not valid for non-polar and polar-aprotic solvent.

Fluorescence emission features assets of the target compounds **5a**-**5g** were investigated in chloroform, ACN, DMF and methanol solvents at ambient temperature as an expressive means of covering examination of electronic relations of the substituted/unsubstituted rhodamine core in the excited state. The fluorescence emission spectra of the target compounds **5a**-**5g** in chloroform, ACN, DMF and methanol solvents (As displayed in Fig. 2A, B, C & D) demonstrates a major specific broad peak varying from 510 to 650 nm, since the transition takes place from higher energy level (excited state) to lower energy level (ground state) transitions i.e. $n^* \rightarrow \pi$ and $\pi^* \rightarrow \pi$. The rhodamine derivatives **5c**, **5d**, **5e** and **5g** exhibit strong fluorescence emission intensity in all solvents nevertheless compounds **5a**, **5b** and **5f** shows less intensity expect in methanol. Also, the relative quantum yield and a fluorescence lifetime values for compounds **5a**, **5b** and **5f** manifest electronic impact of the unsubstituted phenyl ring and ortho-substituted phenyl group (-OH and —F) present in the respective compounds i.e. **5a**, **5b** & **5c** respectively (Table 1 & Fig. 3). This variation might be possibly caused because of the moderately and strongly activating groups (—F, -OCH_3, and -OH) present in respective compounds. In practice, when these substituents are present at ortho/meta/para position or without substituents with respect to the amide functionality, experiences of different electronic effects on the phenyl moiety triggers to deliver variation in the photophysical properties of the respective compounds in various solvents.

Fluorescence spectra of the synthesized derivatives guide us to evaluate the distinct photophysical factors such as, stokes shift, fluorescence quantum yield for each compound in a variety of solvents. In fact, the excellent fluorescent properties or the changeover in spectroscopic properties owing to change in the various polarity of the solvents are the key hypothesis of this experiment. The calculated photophysical parameters, for all the synthesized derivatives in variety of solvents are organized in Tables 1, 2, 3 & 4 separately. The estimated values of the quantum yield suggest that the quantum yield value decreases as the polarity of the solvent increases (except for methanol) owing to the charge transfer phenomenon. In fact, the fluorescence quantum yield values for compound **5a**, **5b**, **5c**, & **5d** increases in polar protic solvent (methanol) because of the negative solvatokinetic effect. Whereas

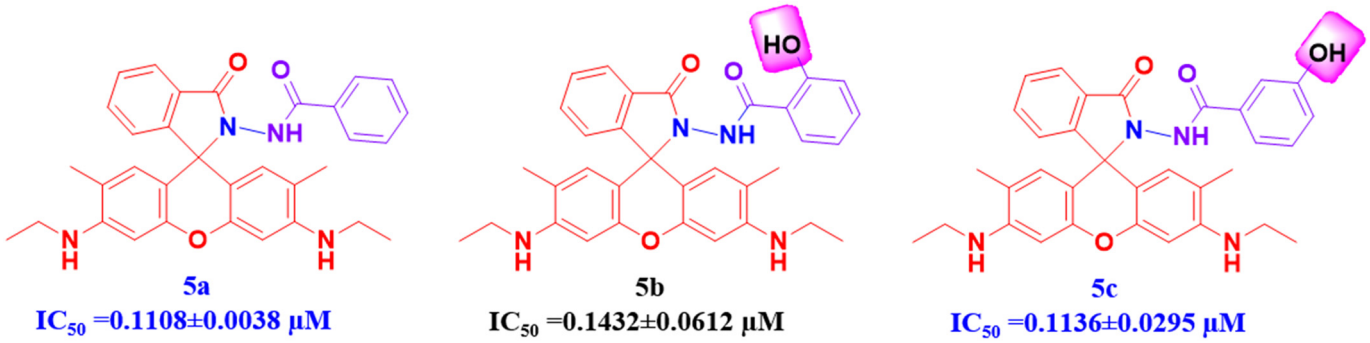

Fig. 3. Structural activity relationship of **5a**, **5b**, and **5c**.

Table 2
In-vitro IC_{50} value for urease inhibition of compounds **5a-5g**.

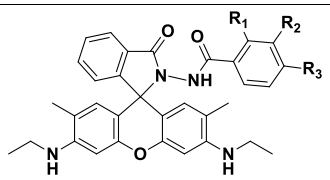

5(a-g)

Sr. no	Compounds	(5a-5g)			Urease activity IC_{50} ± SEM (μM)
		R^1	R^2	R^3	
1	**5a**	**-H**	**-H**	**-H**	**0.1108±0.0038**
2	**5b**	-OH	-H	-H	0.1432±0.0612
3	**5c**	**-H**	**-OH**	**-H**	**0.1136±0.0295**
4	**5d**	-H	$-OCH_3$	-H	0.1456±0.0194
5	**5e**	-H	-H	$-OCH_3$	0.8644±0.0828
6	**5f**	-F	-H	-H	0.1525±0.0201
7	**5g**	-H	-H	-F	0.1489±0.0343
8	**Thiourea**				**4.7201±0.0546**

SEM = Standard error of the mean; values are expressed in mean ± SEM.

Table 3
Kinetic parameters of the jack bean urease for urea activity in the presence of different concentrations of **5a**.

Concentration (μM)	V_{max} (ΔA/min)	K_m (mM)	Inhibition type	*Ki* (μM)
0.00	0.001049091	2	Non-competitive	0.04
0.06	0.000408182	2		
0.12	0.000222481	2		
0.24	0.000139091	2		

Where, V_{max} = velocity of the reaction, K_m = Michaelis-Menten constant, *Ki* = EI dissociation constant.

compound **5e**, **5f**, and **5g** had lower quantum yield values in a highly polar solvent (methanol) equated with the other solvents acquiring less polarity ($CHCl_3$ and ACN) due to the positive solvatokinetic effect [16]. In addition, the present -NH unit transfer an electron towards the xanthene platform leads to an intramolecular charge transfer (ICT) effect to take place [16,66]. Because of the ICT effect, the impact of the solvent polarity upon the emission band was more remarkable compared with the absorption spectra. Furthermore, the dipole moment concurrently increases to solvent molecule in the excited state via relaxation process. The spectral shift is usually dependent upon the change-over in dipole moment and the disparity in dielectric constants of the respective solvents which triggers alteration of fluorescence lifetime values. The lifetime value decrease implies, the decrease in the radiative pathways from the excited state. Hence, the fluorescence lifetime values are also dependent on the dielectric constant, dipole moment and the polarity of the solvents which are used for spectroscopic parameter studies [66,67]. The transformations detected for all the synthesized compounds in various solvents are slight but nevertheless performs a significant function in an excited state phenomenon of the compounds and changes in their spectral assets.

Overall, emission spectra of all the synthesized derivatives are affected by changing the polarity of the solvent. After comparing all the target compounds **5a**-**5g** and their fluorescence emission response in respect to nonpolar (chloroform), polar aprotic (ACN & DMF), and polar protic (methanol) solvent reveals that, the compound **5c** shows

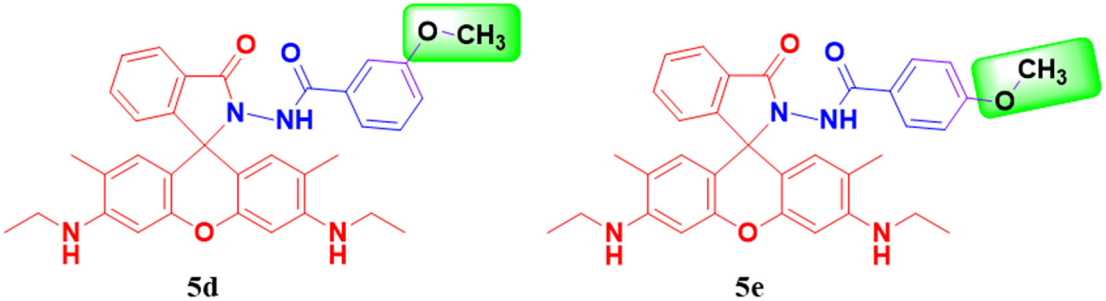

Fig. 4. Structural activity relationship of **5d** and **5e**.

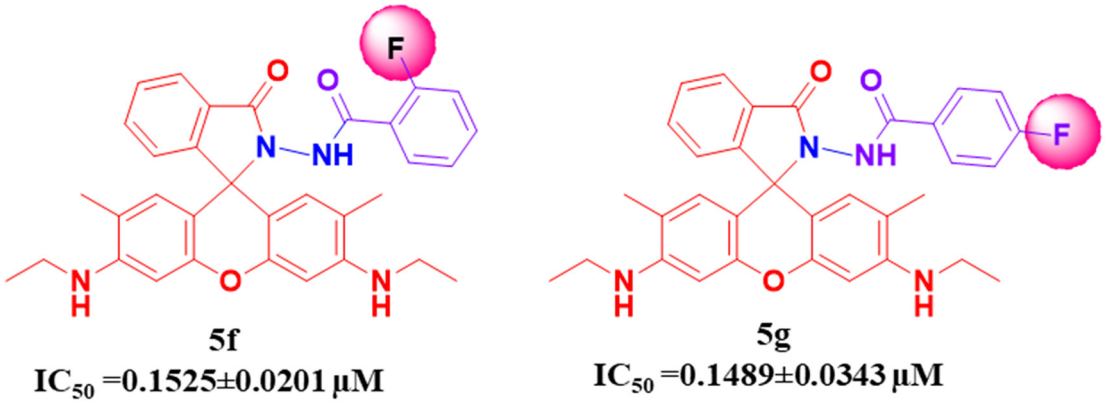

Fig. 5. Structural activity relationship of **5f** and **5g**.

maximum fluorescence emission response along with good photophysical properties equated with the other derivatives (5a, 5b & 5d-5g).

3.2. In vitro urease activity and structural activity relationship (SAR)

A series of the rhodamine-based derivatives (**5a**-**5g**) were synthesized systematically as presented in Scheme 2. The objective behind the new compounds was to synthesize the therapeutically active compounds which can be used in future for the development of a new

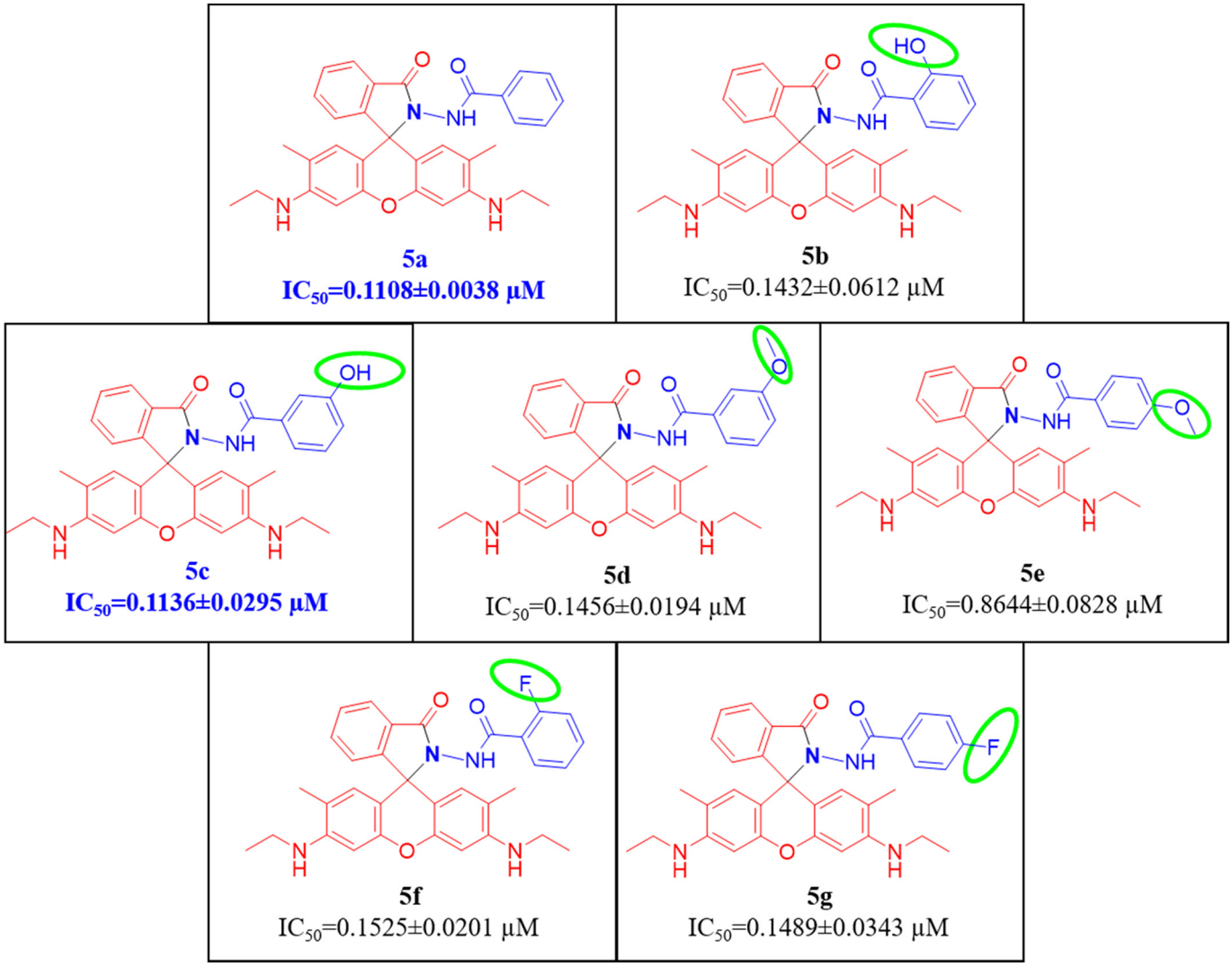

Fig. 6. Structure activity relationship of **5a**-**5g**.

drug. The synthesized target compounds (**5a**-**5g**) were employed for their urease inhibitory activity, as a result fluctuating inhibitory activity was detected with modifying the various substituents and its position on the benzamide functionality within the target compounds. The inhibitory activity ranged from 0.1108 ± 0.0038 to 0.8644 ± 0.0828 μM, all the derivatives display respectable outcome for the urease inhibitory activity but among them compound **5c** (IC_{50} value 0.1108 ± 0.0038 μM) shows most potent activity compared with standard inhibitor thiourea (IC_{50} value 4.7201 ± 0.0546 μM). The results are given in Table 2.

The activity which is observed by the in-vitro study for the compounds (**5a**-**5g**), is all because of the involvement of the whole molecule. Therefore, to scrutinize the importance of the attached different substituent (Such as -OH, $-OCH_3$ or —F) on the activity limited structural activity relationship (SAR) study was employed. Figs. 3–6 display the structure of the different target compounds.

As shown in Fig. 3, among the two hydroxy (-OH) regio-isomers i.e. **5b** and **5c**, the compound containing the hydroxy substituent at meta position i.e. **5c** (IC_{50} = 0.1108 ± 0.0038 μM) displays a decent inhibition than **5b** (IC_{50} = 0.1432 ± 0.0612 μM), in which ortho position occupied by the hydroxy group. Thus, it can be deduced from the in-vitro study that, the inhibition rate decreases when the electron-donating substituents are present at the ortho position. It means the interaction of the meta substituted ligand (**5c**) was more efficient than ortho-substituted ligand (**5b**).

Besides, as displayed in Fig. 4, the hydroxy group (-OH) was superseded by an electron-donating group such as methoxy ($-OCH_3$) at meta and para-position, respectively. The outcomes exhibit that, the meta substituted derivative **5d** (IC_{50} = 0.1456 ± 0.0194 μM) demonstrate higher inhibition than para-substituted derivative **5e** (IC_{50} = 0.8644 ± 0.0828 μM). Yet again, it confirmed that when an electron-donating ($-OCH_3$) substituent was present at meta-position (**5d**) the interaction with the enzyme was more powerful than the para-substituted derivative (**5e**), which cause a decline in the urease inhibitory activity at para-position associated with meta substituted derivatives (Fig. 4).

Likewise, the ortho and para position of the benzamide functionality in the target compounds **5f** (IC_{50} = 0.1525 ± 0.0201 μM) and **5g** (IC_{50} = 0.1489 ± 0.0343 μM) has been replaced by the fluorine (electron donating) group, as presented in Fig. 5. Herein, fluorine donates the lone pair of electrons through resonance which activates the phenyl ring of the benzamide functionality and leads to increases the electron density at ortho and para positions. Therefore, both the target compounds (5f and 5g) appears virtually the same interaction with the enzyme. But among them, the para substituted compound proves decent inhibitory activity as compared to the para-substituted compound. By equating both compounds, the para-substituted compound displays fairly urease inhibitory activity than ortho-substituted due to the fluorine substituents present at ortho position, which is more closer to the carbonyl functionality and have further prospects to generate a steric interaction between them than para substituted fluorine compound **5g**.

Furthermore, the authentication of the impact of the electron-donating substituents on the benzamide functionality present in the target compounds have been demonstrated in the SAR study. Wherein, we have equated numerous substituted target compounds (**5b**, **5c**, **5d**, **5e**, **5f** and **5g**) with the unsubstituted derivative **5a** (**IC_{50} = 0.1108 ± 0.0038 μM**). At this time, it has been remarked that the unsubstituted and meta-substituted compound i.e. **5a** & **5c**, reveal an excellent role as compared not only with the ortho and para substituted target compounds but also with the standard drug thiourea (**IC_{50}** = 4.7201 ± 0.0546 μM) as indicated in Fig. 6 and Table 2.

In summary, while comparing all the derivatives **5a**-**5g**, along with their activity and attachment of the different substituents. The findings have shown that, when an electron-donating substituent like –OH, $-OCH_3$ or —F are present at ortho or para-position, the interaction of the enzyme was not efficient compared with the meta substituted derivatives. It is well understood that the electron-donating are ortho/para directing in aromatic benzene ring. Therefore, it suggests that the substituents that appear at ortho/para position could be more sensible to enhance the conjugation along with the benzamide carbonyl moiety, which causes to decrease the interaction with an enzyme, as a result, decrease the urease inhibitory activity. Whereas, in the case of meta-substitution, the conjugation phenomenon along with carbonyl functionality is absent and causes to increases the rate of the inhibition compared with the ortho and para-substituted derivatives. Likewise, there will be no more potential in the benzamide functional group to enhance the electron density of the phenyl ring in the absence of the substituents. Hence, this may lead to increase in the effectual interaction between the energetic site of the enzyme and the unsubstituted ligand **5a** causes it to increase the urease inhibitory activity.

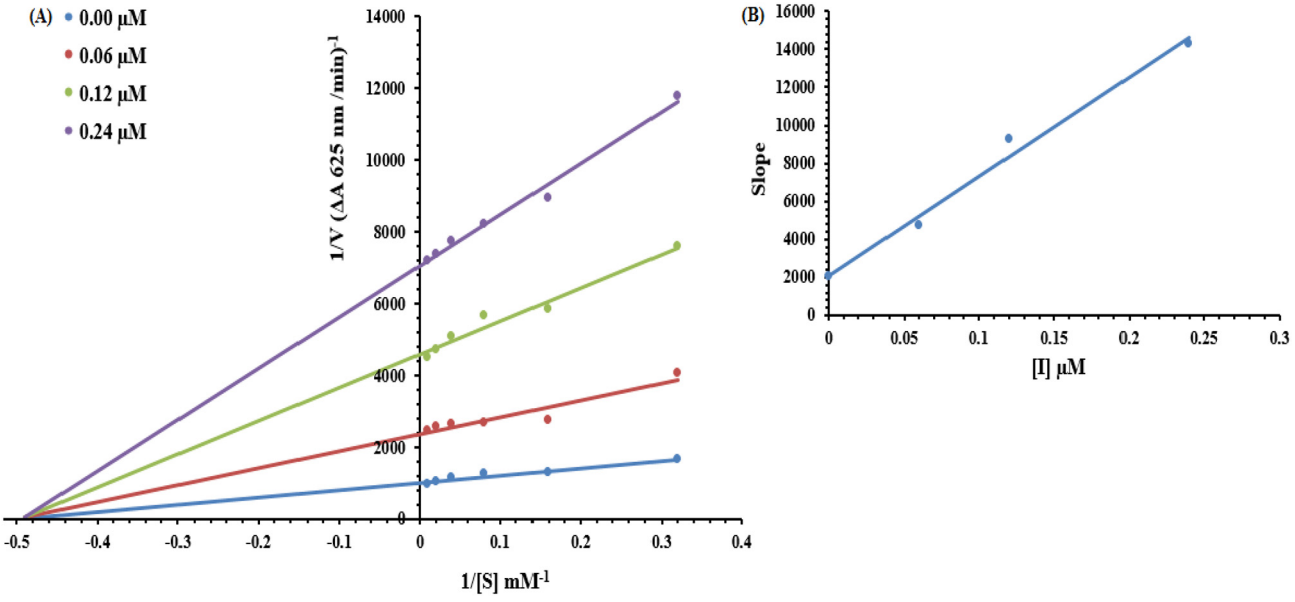

Fig. 7. Lineweaver–Burk plots for inhibition of Urease in the presence of compound **5a**. (A) Concentrations of **5a** were 0.00, 0.06, 0.12 and 0.24 μM. (B) The insets represent the plot of the slope or the vertical versus inhibitor **5a** concentrations to determine inhibition constants. The lines were drawn using linear least squares fit.

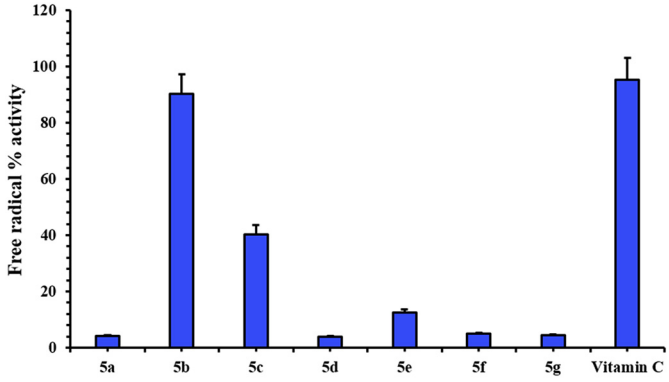

Fig. 8. Free radical % scavenging activity of synthetic compounds values were represented as mean ± SEM (Standard error of the mean). All compounds concentrations were 100 μg/mL.

Therefore, it was determined from structural activity relationships that, if the electron-donating groups were present at ortho or para-position, the interaction with enzyme was not as effective as with the meta-substituted derivatives, but it was more operative in absence of the electron-donating groups. The xanthene derivatives **5a**-**5g** can be arranged as per trend observed in in-vitro study: **5a** > **5c** > **5b** > **5d** > **5g** > **5f** > **5e**.

3.3. In vitro analysis:

3.3.1. Kinetic analysis

To estimate the sort of inhibition and inhibition constant on jack bean urease, compound **5a** was chosen for further study as per our obtained result. In terms of EI (Enzyme inhibitor) and ESI (Enzyme Substrate Inhibitor) constants, the potential of the synthesized compounds to inhibit free enzyme and enzyme-substrate complexes was determined. The Lineweaver-Burk graph of 1/V against 1/[S] plotted (where, 'V' is the velocity of reaction and 'S' is the reaction of substrate) in the existence of discrete compounds in enzyme kinetic experiments was employed. This shows a series of straight lines (Fig. 7A). From the outcome it was observed that within the second quadrant the compound **5a** was intersected. Besides, the analysis displays the value of V_{max} decreases with increase in the inhibitor doses but on the other hand, the K_m remains constant. This behaviour indicates that compound **5a** inhibits the urease non-competitively to form the enzyme inhibitor complex. The Secondary plot of slope against the concentration of inhibitors displayed enzyme inhibitor dissociation constant (K*i*) (Fig. 7B). The kinetic results are presented in Table 3.

3.3.2. Free radical scavenging activity

All the synthesized compounds (**5a**-**5g**) were evaluated for DPPH free radical scavenging ability. In the comparison of the standard, the compound **5b** showed an excellent activity other than all the synthesized compounds which did not show significant activity, even at high concentration (100 μg/mL). Vitamin C was used as a reference drug. The results are presented in Fig. 8.

3.4. In silico analysis

3.4.1. Structural and physicochemical evaluation of Jack bean urease

Jack bean urease is a class of metal-containing hydrolase protein consisting of four domains with distinct residue numbers. The VADAR assessment exhibited that the structure of the protein contained 27% helices, 31% β sheets and 41% coils in the target protein. In addition, Ramachandran plots stated that 97.5% of the residues were present in

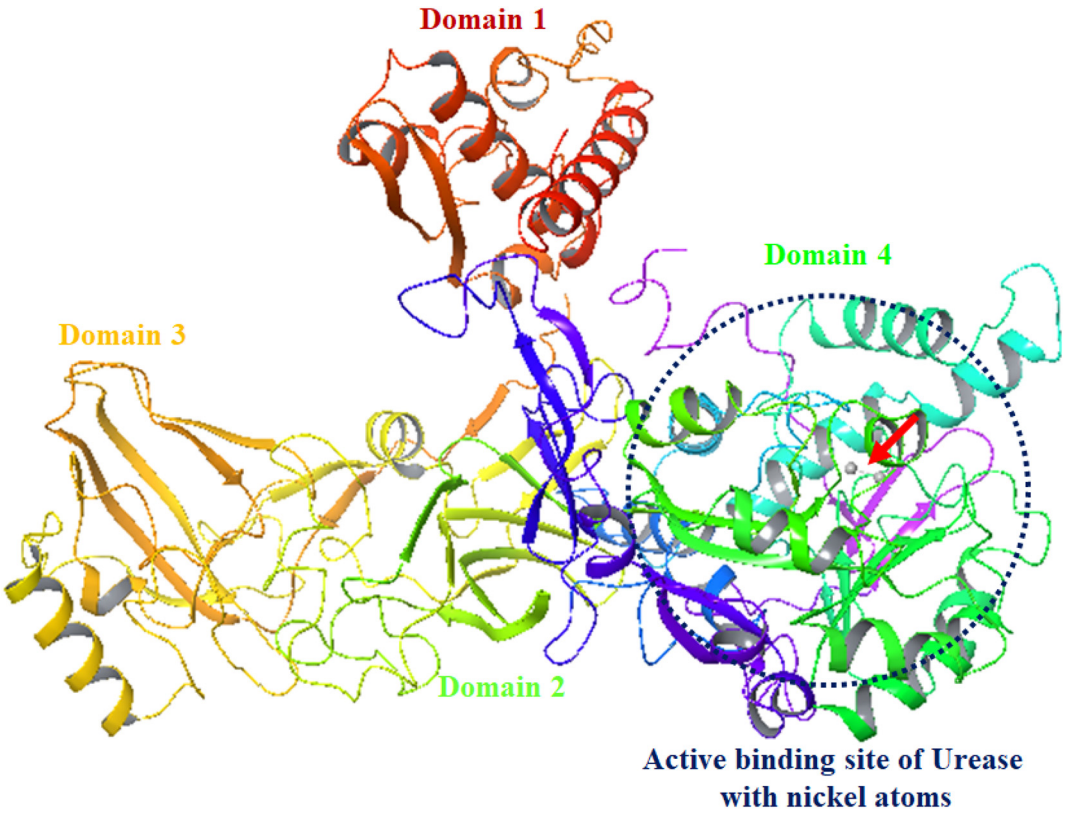

Fig. 9. The overall protein structure of jack bean urease.

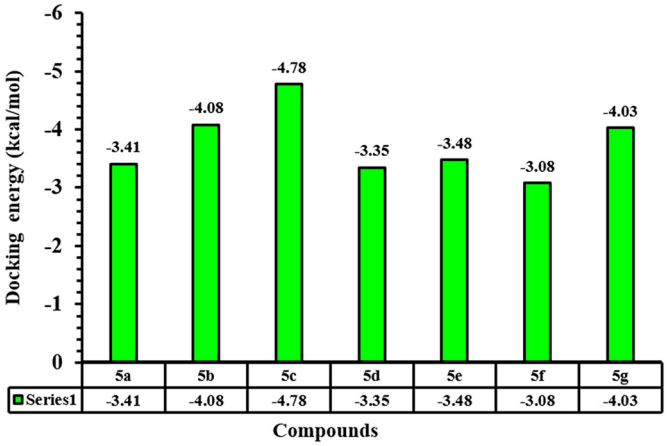

Fig. 10. Docking energy values of ligands.

preferred areas, showing the accuracy of the corners of phi (φ), and psi (ψ) angles among the jack bean urease coordinates. The overall protein structure is mentioned in Fig. 9.

3.4.2. Binding energy evaluation of the synthesized compounds

To forecast the best-fitted conformational site of the synthesized compounds (**5a**-**5g**), the compounds were docked against jack bean urease. The generated docked complexes were examined based on glide docking energy values (kcal/mol) and bonding interaction (hydrogen/hydrophobic) pattern. The binding energy value depicts the conformational position within the active region of the target protein. The docking results show that **5c** showed higher energy value (−4.78 kcal/mol) compared to other ligands. The binding difference was not much fluctuated among all the docking energy score as the basic ligand skeleton was similar in all synthetic compounds. The other compounds possessed different energy values such as −3.41, −4.08, −3.35, −3.48, −3.08 and −4.03 kcal/mol (Fig. 10) [26,56].

3.4.3. Ligand-binding analysis of urease docked complexes

Molecular docking approach is one of the most significant approach to understand and visualize the binding interaction outline of designed ligands against target protein structure [68]. Based on in-vitro results (IC_{50}) **5a** was selected for close binding interaction pattern. In detailed binding analysis, single π-π interaction was observed in **5a** docking complex. The benzene ring structure of **5a** forms π-π interaction with Arg639. The other residues which are in close contact with the ligand structure are Ile411, Leu415, Glu418, Arg439, Gln635, Met635, Gly638, Val640, Pro573 and Met588. These amino acids are core binding pocket residues and prior docking research data ensured the importance of these residues in bonding with other urease inhibitors, which strengthen our docking results [52,69]. The comparative SAR analysis showed the significance of **5a** might be considered as potent inhibitor by targeting jack bean urease. The three-dimensional (3D) docking graphical depiction for **5a** is mentioned in Fig. 11 and all other ligands 2D docking images are justified in Fig. 12.

4. Conclusion

Novel xanthene related derivatives **5a**-**5g** have been synthesized and well-characterized by using FT-IR, LC-MS, ^{1}H NMR and ^{13}C NMR. The photophysical properties such as, absorption and emission wavelengths, molar absorptivity, stokes shift, fluorescence quantum yield and fluorescence lifetime values, were assessed in various solvents by using absorption and fluorescence virtual study. All compounds exhibited substantial fluorescent properties as equating to the polarity of the solvents. Although, it was found that compound **5c** exhibited astonishing fluorogenic performance as well as high fluorescence quantum yield and fluorescence lifetime results among all the derivatives. Moreover, all the target compounds **5a**-**5g** were screened against jack bean urease inhibition and antioxidant activity to understand the crucial function of the effective enzyme inhibitors. Among all the derivatives, compound **5a** (IC_{50} = 0.1108 ± 0.0038 μM) and **5c** (IC_{50} = 0.1136 ± 0.0295) displayed admirable inhibitory activity even if an equated with the standard drug thiourea having IC_{50} value 4.7201 ± 0.0546 μM. Likewise, compounds **5a**-**5g** were examined counter to DPPH free radical scavenging activity in which, compound **5b** & **5c** proved exceptional an antioxidant activity relative to other derivatives. In addition, the survey of molecular docking analysis is in favour of the in-vitro study. Overall, the current research work not only aims to synthesize and investigate the optical properties of the novel xanthene derivatives but also operate as a significant jack bean urease

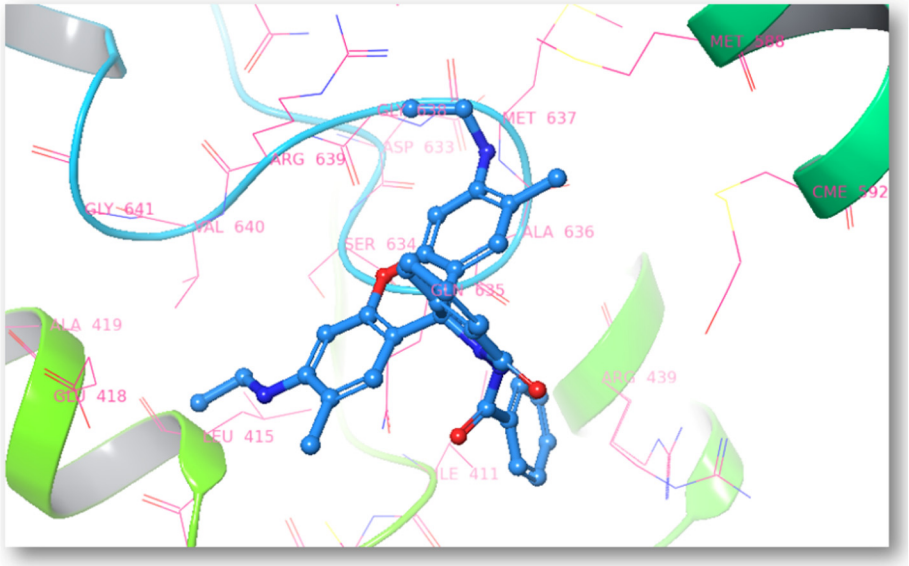

Fig. 11. Binding pocket of urease protein.

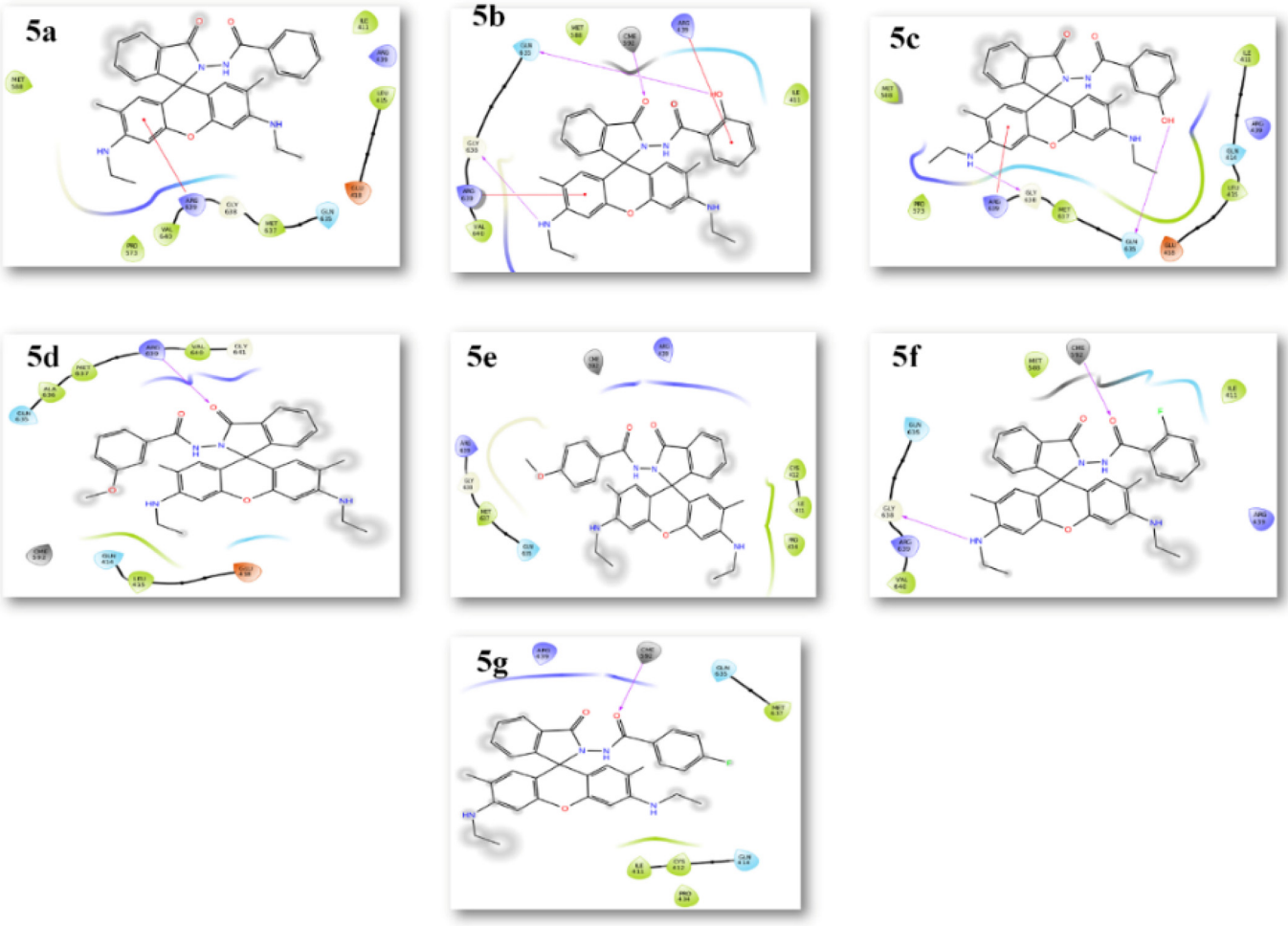

Fig. 12. Docking complexes of ligands **5a**-**5g**.

inhibitors. Also, in future these compounds **5a**-**5g** can be used in various applications such as biomarker in cell imaging, chemosensor for the detection of metal ions or in drug design field for the development of potent urease inhibitor against jack bean urease.

CRediT authorship contribution statement

Balasaheb D. Vanjare: Conceptualization, Formal analysis, Writing - original draft, Writing - review & editing. **Prasad G. Mahajan:** Writing - original draft. **Nilam C. Dige:** Writing - original draft. **Hussain Raza:** Formal analysis, Writing - review & editing. **Mubashir Hassan:** Formal analysis, Writing - review & editing. **Sung-Yum Seo:** Conceptualization, Writing - review & editing. **Ki Hwan Lee:** Conceptualization, Formal analysis, Writing - review & editing.

Declaration of competing interest

Authors declare no conflict of interest.

Acknowledgment

This research was supported by Basic Science Research Program through the National Research Foundation of Korea (NRF) funded by the Ministry of Education (NRF-2019R1I1A3A01059089).

Appendix A. Supplementary data

Supplementary data to this article can be found online at https://doi.org/10.1016/j.saa.2020.118667.

References

[1] Y. Koide, Y. Urano, K. Hanaoka, T. Terai, T. Nagano, Development of an Si-rhodamine-based far-red to near-infrared fluorescence probe selective for hypochlorous acid and its applications for biological imaging, J. Am. Chem. Soc. 133 (2011) 5680–5682, https://doi.org/10.1021/ja111470n.

[2] B.D. Vanjare, P.G. Mahajan, N.C. Dige, A.R. Phull, S.J. Kim, K.H. Lee, Synthesis and studies on photophysical properties of rhodamine derivatives for bioimaging applications, B. K. C. S. 40 (2019) 554–559, https://doi.org/10.1002/bkcs.11733.

[3] S. Kenmoku, Y. Urano, H. Kojima, T. Nagano, Development of a highly specific rhodamine-based fluorescence probe for hypochlorous acid, and its application to real-time imaging of phagocytosis, J. Am. Chem. Soc. 129 (2007) 7313–7318, https://doi.org/10.1021/ja068740g.

[4] Y.Q. Sun, J. Liu, X. Lv, Y. Liu, Y. Zhao, W. Guo, Rhodamine-inspired far-red to near-infrared dyes and their application as fluorescence probes, Angew. Chem. Int. Ed. 51 (2012) 7634–7636, https://doi.org/10.1002/anie.201202264.

[5] Y.K. Yang, K.J. Yook, J.A. Tae, Rhodamine-based fluorescent and colorimetric chemodosimeter for the rapid detection of Hg^{2+} ions in aqueous media, J. Am. Chem. Soc. 127 (2005) 16760–16761, https://doi.org/10.1021/ja054855t.

[6] P. Mahato, S. Saha, E. Suresh, R.D. Liddo, P.P. Parnigotto, M.T. Conconi, M.K. Kesharwani, B. Ganguly, A. Das, Ratiometric detection of Cr^{3+} and Hg^{2+} by a naphthalimide-rhodamine based fluorescent probe, Inorg. Chem. 51 (2012) 1769–1777, https://doi.org/10.1021/ic202073q.

[7] J. Chen, W. Liu, B. Zhou, G. Niu, H. Zhang, J. Wu, Y. Wang, W. Ju, P. Wang, Coumarin- and rhodamine-fused deep red fluorescent dyes: synthesis, photophysical properties, and bioimaging in vitro, J. Organomet. Chem. 78 (2013) 6121–6130, https://doi.org/10.1021/jo400783x.

[8] M. Saleem, K.H. Lee, Selective fluorescence detection of Cu^{2+} in aqueous solution and living cells, J. Lumin. 145 (2014) 843–848, https://doi.org/10.1016/j.jlumin.2013.08.044.

[9] N. Uchida, J. Combs, S. Chen, E. Zanjani, R. Hoffman, A. Tsukamoto, Primitive human hematopoietic cells displaying differential efflux of the rhodamine 123 dye have distinct biological activities, Blood. 88 (1996) 1297–1305.

[10] H. Wang, L. Lu, S. Zhu, Y. Li, W. Cai, The Phototoxicity of xanthene derivatives against Escherichia coli, Staphylococcus aureus, and Saccharomyces cerevisiae, Curr. Microbiol. 52 (2006) 1–5, https://doi.org/10.1007/s00284-005-0040-z.

[11] R. Bucki, J.J. Pastore, P. Randhawa, R. Vegners, D.J. Weiner, P.A. Janmey, Antibacterial activities of rhodamine B-conjugated gelsolin-derived peptides compared to those of the antimicrobial peptides cathelicidin LL37, magainin II, and melittin, Antimicrob. Agents Chemother. 48 (2004) 1526–1533.

[12] M. Kaya, E. Demir, H. Bekci, Synthesis, characterization, and antimicrobial activity of novel xanthene sulfonamide and carboxamide derivatives, J. Enzyme Inhib. Med. Chem. 28 (2013) 885–893, https://doi.org/10.3109/14756366.2012.692087.

[13] J. Chen, W. Liu, B. Zhou, G. Niu, H. Zhang, J. Wu, Y. Wang, W. Ju, P. Wang, Coumarin- and rhodamine-fused deep red fluorescent dyes: synthesis, photophysical properties, and bioimaging in vitro, J. Organomet. Chem. 78 (2013) 6121–6130, https://doi.org/10.1021/jo400783x.

[14] P.C. Beaumont, D.G. Johnson, B.J. Parsons, Photophysical properties of laser dyes: picosecond laser flash photolysis studies of rhodamine 6G, rhodamine B and rhodamine 101, J. Chem. Faradays Trans. 89 (1993) 4185–4191.

[15] M. Savarese, A. Aliberti, I.D. Santo, E. Battista, F. Causa, P.A. Netti, N. Rega, Fluorescence lifetimes and quantum yields of rhodamine derivatives: new insights from theory and experiment, J. Phys. Chem. A 116 (2012) 7491–7497, https://doi.org/10.1021/jp3021485.

[16] E. Bozkurta, H.I. Gulb, E. Mete, Solvent, and substituent effect on the photophysical properties of pyrazoline derivatives: a spectroscopic study, J. Photochem. Photobiol. A Chem. 352 (2018) 35–42, https://doi.org/10.1016/j.jphotochem.2017.10.010.

[17] M. Saleem, K.H. Lee, Selective fluorescence detection of Cu_2p in aqueous solution and living cells, J. Lumin. 145 (2014) 843–848, https://doi.org/10.1016/j.jlumin.2013.08.044.

[18] a) P.G. Mahajan, N.C. Dige, B.D. Vanjare, E. Kamaraj, S.Y. Seo, K.H. Lee, Nano molar level chromogenic and fluorogenic sensing of heavy metal ions using multi-responsive novel Schiff base as a dual mode chemosensor, J. Photochem. Photobiol. A Chem. 385 (2019) 112089, https://doi.org/10.1016/j.jphotochem.2019.112089;
b) B.D. Vanjare, P.G. Mahajan, S.K. Hong, K.H. Lee, Discriminating chemosensor for detection of Fe^{3+} in aqueous media by fluorescence quenching methodology, Bull. Kor. Chem. Soc. 39 (2018) 631–637, https://doi.org/10.1002/bkcs.11442.

[19] S. Yasuhiko, Organic materials for electronic and optoelectronic devices, J. Mater. Chem. 10 (2000) 1–25, https://doi.org/10.1039/A908130E.

[20] W.Z. Yuan, Y. Gong, S. Chen, X.Y. Shen, J.W.Y. Lam, P. Lu, Y. Lu, Z. Wang, R. Hu, N. Xie, H.S. Kwok, Y. Zhang, J.Z. Sun, B.Z. Tang, Efficient solid emitters with aggregation-induced emission and intramolecular charge transfer characteristics: molecular design, synthesis, photophysical behaviors, and OLED application, Chem. Mater. 24 (2012) 1518–1528, https://doi.org/10.1021/cm300416y.

[21] A. Saeed, S.U. Rehma, P.A. Channar, F.A. Larik, Q. Abbas, M. Hassan, H. Raza, U. Florke, S.Y. Seo, Long chain 1-acyl-3-arylthioureas as jack bean urease inhibitors, synthesis, kinetic mechanism and molecular docking studies, J. Taiwan. Inst. Chem. E. 77 (2017) 54–63, https://doi.org/10.1016/j.jtice.2017.04.044.

[22] M.A. Abbasi, M. Hassan, A.U. Rehman, S.Z. Siddiqui, H. Raza, S.A. Shah, S.Y. Seo, Synthesis, in vitro and in silico studies of novel potent urease inhibitors: N-[4-({5-[(3-un/substituted-anilino-3-oxopropyl) sulfanyl]-1,3,4- oxadiazo2-yl} methyl)-1,3-thiazol-2-yl] benzamides, Bioorg. Med. Chem. 26 (2018) 3791–3804, https://doi.org/10.1016/j.bmc.2018.06.005.

[23] M.A. Abbasi, H. Raza, A.U. Rehman, S.Z. Siddiqui, S.A.A. Shah, M. Hassan, S.Y. Seo, Synthesis of novel N-(1,3-thiazol-2-yl) benzamide clubbed oxadiazole scaffolds: urease inhibition, Lipinski rule and molecular docking analyses, Bioorg. Chem. 83 (2019) 63–75, https://doi.org/10.1016/j.bioorg.2018.10.018.

[24] L.S.B. Upadhyay, Urease inhibitors: a review, Indian J. Biotechnol. 11 (2012) 381–388http://nopr.niscair.res.in/handle/123456789/15679.

[25] B.D. Vanjare, P.G. Mahajan, M. Hassan, H. Raza, S.Y. Seo, S.K. Hong, K.H. Lee, Synthesis, photophysical properties, biological estimation and molecular docking studies of novel schiff base derivatives as potential urease inhibitors, J. Fluoresc. 28 (2018) 1295–1304, https://doi.org/10.1007/s10895-018-2289-1.

[26] P.G. Mahajan, N.C. Dige, B.D. Vanjare, H. Raza, M. Hassan, S.Y. Seo, S.K. Hong, K.H. Lee, Synthesis and studies of fluorescein based derivatives for their optical properties, urease inhibition and molecular docking, J. Fluoresc. 28 (2018) 1305–1315, https://doi.org/10.1007/s10895-018-2291-7.

[27] Y.F. Rego, M.P. Queiroz, T.O. Brito, P.G. Carvalho, V.T. Queiroz, A. Fátima, F.A. Macedo, Review on the development of urease inhibitors as antimicrobial agents against pathogenic bacteria, J. Adv. Res. 13 (2018) 69–100, https://doi.org/10.1016/j.jare.2018.05.003.

[28] A.D. Fatima, C.D.P. Pereira, C.R. Olímpio, B.G. Oliveira, L.L. Franco, P.H. Silva, Schiff bases and their metal complexes as urease inhibitors – a brief review, J. Adv. Res. 13 (2018) 113–126, https://doi.org/10.1016/j.jare.2018.03.007.

[29] A. Khan, J. Hashim, N. Arshad, I. Khan, N. Siddiqui, A. Wadood, M. Ali, F. Arshad, K.M. Khan, M.I. Choudhary, Dihydropyrimidine based hydrazine dihydrochloride derivatives as potent urease inhibitors, Bioorg. Chem. 64 (2016) 85–96, https://doi.org/10.1016/j.bioorg.2015.12.007.

[30] K.M. Khan, F. Rahim, A. Khan, M. Shabeer, S. Hussain, W. Rehman, M. Taha, M. Khan, S. Perveen, M.I. Choudhary, Synthesis and structure–activity relationship of thiobarbituric acid derivatives as potent inhibitors of urease, Bioorg. Med. Chem. 22 (2014) 4119–4123, https://doi.org/10.1016/j.bmc.2014.05.057.

[31] M. Saleem, M. Rafiq, Y.K. Jeong, D.W. Cho, C.H. Kim, S.Y. Seo, C.A.S. Choi, S.K. Hong, K.H. Lee, Facile synthesis, crystal structure, DFT calculation and biological activities of 4-(2-fluorophenyl)-3-(3-methoxybenzyl)-1H-1,2,4-triazol-5(4H)-one (5), Med. Chem. 14 (2018) 451–459, https://doi.org/10.2174/1573406414666180112122856.

[32] M.A.S. Aslam, S.U. Mahmood, M. Shahid, A. Saeed, J. Iqbal, Synthesis, biological assay in vitro and molecular docking studies of new Schiff base derivatives as potential urease inhibitors, Eur. J. Med. Chem. 46 (2011) 5473–5479, https://doi.org/10.1016/j.ejmech.2011.09.009.

[33] M. Hanif, M. Saleem, M.T. Hussain, N.H. Rama, S. Zaib, M.A. Aslam, P.G. Jones, J. Iqbal, Synthesis, urease inhibition, antioxidant and antibacterial studies of some 4-amino-5-aryl-3H-1,2,4-triazole-3-thiones and their 3,6-disubstituted 1,2,4-triazolo[3,4-b] 1,3,4-thiadiazol derivatives, J. Braz. Chem. Soc. 23 (2012) 854–860, https://doi.org/10.1590/S0103-50532012000500010.

[34] E. Menteşe, H. Bektaş, B.B. Sokmen, M. Emirik, D. Çakır, B. Kahveci, Synthesis and molecular docking study of some 5,6-dichloro-2-cyclopropyl-1H benzimidazole derivatives bearing triazole, oxadiazole, and imine functionalities as potent inhibitors of urease, Bioorg. Med. Chem. Lett. 27 (2017) 3014–3018, https://doi.org/10.1016/j.bmcl.2017.05.019.

[35] B. Zerner, Recent advances in the chemistry of an old enzyme, urease, Bioorg. Chem. 19 (1991) 116–131, https://doi.org/10.1016/0045-2068(91)90048-T.

[36] P. Kafarski, M. Talma, Recent advances in design of new urease inhibitors: a review, J. Adv. Res. 13 (2018) 101–112, https://doi.org/10.1016/j.jare.2018.01.007.

[37] R.K. Andrews, A. Dexter, R.L. Blakeley, B. Zerner, Jack bean urease (EC3.5.1.5.). On inhibition of urease by amides and esters of phosphoric acid, J. Am. Chem. Soc. 108 (1986) 7124–7125.

[38] J.B. Sumner, The isolation, and crystallization of the enzyme urease, J. Biol. Chem. 69 (1926) 435–441.

[39] A. Rauf, S. Shahzad, M. Bajda, M. Yar, F. Ahmed, N. Hussain, N.M. Akhtar, A. Khan, J. Ionczyk, Design and synthesis of new barbituric- and thiobarbituric acid derivatives as potent urease inhibitors: structure activity relationship and molecular modelling studies, Bioorg. Med. Chem. 23 (2015) 6049–6058, https://doi.org/10.1016/j.bmc.2015.05.038.

[40] H. Cantarella, R. Otto, J.R. Soares, A.G.D.B. Silva, Agronomic efficiency of NBPT as a urease inhibitor: a review, J. Adv. Res. 13 (2018) 19–27, https://doi.org/10.1016/j.jare.2018.05.008.

[41] L.V. Modolo, C.J.D. Silva, D.S. Brandão, I.S.A. Chaves, Minireview on what we have learned about urease inhibitors of agricultural interest since mid-2000s, J. Adv. Res. 13 (2018) 29–37, https://doi.org/10.1016/j.jare.2018.04.001.

[42] F. Iftikhar, Y. Ali, F.A. Kiani, S.F. Hassan, T. Fatima, A. Khan, B. Niaz, A. Hassan, F.L. Ansari, U. Rashid, Design, synthesis, in vitro evaluation and docking studies on dihydropyrimidine based urease inhibitors, Bioorg. Chem. 74 (2017) 53–65, https://doi.org/10.1016/j.bioorg.2017.07.003.

[43] A. Saeed, M.S. Khan, H. Rafique, M. Shahid, J. Iqbal, Design, synthesis, molecular docking studies and in vitro screening of ethyl 4-(3-benzoylthioureido) benzoates as urease inhibitors, Bioorg. Chem. 52 (2014) 1–7, https://doi.org/10.1016/j.bioorg.2013.10.001.

[44] U. Rashid, F. Rahim, M. Taha, M. Arshad, H. Ullah, T. Mahmood, M. Ali, Synthesis of 2-acylated and sulfonated 4-hydroxycoumarins: in vitro urease inhibition and molecular docking studies, Bioorg. Chem. 66 (2016) 111–116, https://doi.org/10.1016/j.bioorg.2016.04.005.

[45] I. Khan, S. Ali, S. Hameed, N.H. Rama, M.T. Hussain, A. Wadood, R. Uddin, Z. Ul-Haq, A. Khan, S. Ali, M.I. Choudhary, Synthesis, antioxidant activities and urease inhibition of some new 1,2,4-triaz and 1,3,4-thiadiazole derivatives, Eur. J. Med. Chem. 45 (2010) 5200–5207, https://doi.org/10.1016/j.ejmech.2010.08.034.

[46] H.Q. Li, Z.P. Xiao, Yin-Luo, T. Yan, P.C. Lv, H.L. Zhu, Amines and oximes derived from deoxybenzoins as Helicobacter pylori urease inhibitors, Eur. J. Med. Chem. 44 (2009) 2246–2251, https://doi.org/10.1016/j.ejmech.2008.06.001.

[47] O.U. Abid, T.M. Babar, F.I. Ali, S. Ahmed, A. Wadood, N.H. Rama, R. Uddin, Zaheer-Ul-Haq, A. Khan, M.I. Choudhary, Identification of novel urease inhibitors by high-throughput virtual and in vitro screening, ACS Med. Chem. Lett. 1 (2010) 145–149, https://doi.org/10.1021/ml100068u.

[48] S. Benini, W.R. Rypniewski, K.S. Wilson, S. Mangani, S. Ciurli, Molecular details of urease inhibition by boric acid: insights into the catalytic mechanism, J. Am. Chem. Soc. 126 (2004) 3714–3715, https://doi.org/10.1021/ja049618p.

[49] A. Hameed, K.M. Khan, S.T. Zehra, R. Ahmed, Z. Shafiq, S.M. Bakht, M. Yaqub, M. Hussain, A.L. León, N. Furtmann, J. Bajorath, H.A. Shad, M.N. Tahir, J. Iqbal, Synthesis, biological evaluation and molecular docking of N-phenyl thiosemicarbazones as urease inhibitors, J. Bioorg. Chem. 61 (2015) 51–57, https://doi.org/10.1016/j.bioorg.2015.06.004.

[50] a W.K. Shi, R.C. Deng, P.F. Wang, Q.Q. Yu, Q. Liu, K.L. Ding, M.H. Yang, H.Y. Zhang, S.H. Gong, M. Deng, W.R. Liu, Q.J. Feng, Z.P. Xiao, H.L. Zh, 3-Arylpropionylhydroxamic acid derivatives as Helicobacter pylori urease inhibitors: synthesis, molecular docking and biological evaluation, Bioorg. Med. Chem. 24 (2016) 4519–4527, https://doi.org/10.1016/j.bmc.2016.07.052;
b B.D. Vanjare, P.G. Mahajan, N.C. Dige, H. Raza, M. Hassan, Y. Han, S.J. Kim, S.Y. Seo, K.H. Lee, Novel 1,2,4-triazole analogues as mushroom tyrosinase inhibitors: synthesis, kinetic mechanism, cytotoxicity and computational studies, Mol. Divers. (2020)https://doi.org/10.1007/s11030-020-10102-5;
c C.W. Cheung, M.L. Ploeger, X. Hu, Direct amidation of esters with nitroarenes, Nat. Commun. (2017)https://doi.org/10.1038/ncomms14878.

[51] A.R. Phull, M. Hassan, Q. Abbas, H. Raza, I.U. Haq, S.Y. Seo, S.J. Kim, In-vitro, in silico elucidation of anti urease activity, kinetic mechanism and COX-2 inhibitory efficacy of coagulansin A of Withania coagulans, Chem. Biodivers. 15 (2018), e1700427. https://doi.org/10.1002/cbdv.201700427.

[52] T.A. Fattah, A. Saeed, P.A. Channar, Z. Ashraf, Q. Abbas, M. Hassan, F.A. Larik, Synthesis, enzyme inhibitory kinetics, and computational studies of novel 1-(2-(4-isobutyl

phenyl) propanoyl)-3-arylthioureas as Jack bean urease inhibitors, Chem. Biol. Drug Des. 91 (2018) 434–447, https://doi.org/10.1111/cbdd.13090.

[53] H. Raza, Q. Abbas, M. Hassan, S.H. Eo, Z. Ashraf, D. Kim, A.R. Phull, S.J. Kim, S.K. Kang, S.Y. Seo, Isolation, characterization, and in-silico, in -vitro and in-vivo antiulcer studies of iso imperator in crystallized from Ostericum koreanum, Pharm. Biol. 55 (2017) 218–226, https://doi.org/10.1080/13880209.2016.1257641.

[54] M.W. Weatherburn, Phenol-hypochlorite reaction for determination of ammonia, J. Anal. Chem. 39 (1967) 971–974.

[55] A. Saeed, P.A. Mahesar, A. Channar, F.A. Larik, Q. Abbas, M. Hassan, H. Raza, S.Y. Seo, Hybrid pharmacophoric approach in the design and synthesis of coumarin linked pyrazolinyl as urease inhibitors, kinetic mechanism and molecular docking, Chem. Biodivers. 14 (2017), e1700035. https://doi.org/10.1002/cbdv.201700035.

[56] P.A. Channar, A. Saeed, F. Albericio, F.A. Larik, Q. Abbas, M. Hassan, H. Raza, S.Y. Seo, Sulfonamide-linked ciprofloxacin, sulfadiazine and amantadine derivatives as a novel class of inhibitors of jack bean urease; synthesis, kinetic mechanism and molecular docking, Molecules 22 (2017) 1352, https://doi.org/10.3390/molecules22081352 (1-20).

[57] A. Saeed, F.A. Larik, P.A. Channar, H. Mehfooz, M.H. Ashraf, Q. Abbas, M. Hassan, S.Y. Seo, An expedient synthesis of N-(1-(5-mercapto-4-((substituted benzylidene) amino)-4H-1,2,4-triazol-3-yl)-2-phenylethyl) benzamides as Jack bean urease inhibitors and free radical scavengers; kinetic mechanism and molecular docking studies, Chem. Biol. Drug Des. 90 (2017) 764–777, https://doi.org/10.1111/cbdd.12998.

[58] C.V.K. Reddy, D. Sreeramulu, M. Raghunath, Antioxidant activity of fresh and dry fruits commonly consumed in India, Food Res. Int. 43 (2010) 285–288, https://doi.org/10.1016/j.foodres.2009.10.006.

[59] Z. Ashraf, M. Rafiq, S.Y. Seo, M.M. Babar, Synthesis, kinetic mechanism, and docking studies of vanillin derivatives as inhibitors of mushroom tyrosinase, Bioorg. Med. Chem. 23 (2015) 5870–5880, https://doi.org/10.1016/j.bmc.2015.06.068.

[60] Schrödinger Release 3, Maestro, 2018, Schrödinger, LLC, New York, NY, 2018.

[61] M.A. Abbasi, H. Raza, A.U. Rehman, S.Z. Siddiqui, M. Nazir, A. Mumtaz, S.A.A. Shah, S.Y. Seo, M. Hassan, Synthesis, antioxidant and in-Silico studies of potent urease inhibitors: N-(4-{[(4-methoxyphenethyl)-(substituted)amino] sulfonyl} phenyl) acetamides, Drug Res. (Stuttg). 69 (2018) 111–120, https://doi.org/10.1055/a-0654-5074.

[62] M. Nazir, M.A. Abbasi, A.U. Rehman, S.Z. Siddiqui, H. Raza, M. Hassan, S.A.A. Shah, M. Shahid, S.Y. Seo, Novel indole-based hybrid oxadiazole scaffolds with N-(substituted-phenyl) butanamides: synthesis, line weaver–burk plot evaluation and binding analysis of potent urease inhibitors, RSC Adv. 8 (2018) 25920–25931, https://doi.org/10.1039/c8ra04987d.

[63] R.A. Friesner, R.B. Murphy, M.P. Repasky, L.L. Frye, J.R. Greenwood, T.A. Halgren, P.C. Sanschagrin, D.T. Mainz, Extra precision glide: docking and scoring incorporating a model of hydrophobic enclosure for protein-ligand complexes, J. Med. Chem. 49 (2006) 6177–6196, https://doi.org/10.1021/jm051256o.

[64] R. Farid, T. Day, R.A. Friesner, R.A. Pearlstein, New insights about HER blockade obtained from protein modelling, potential energy mapping, and docking studies, Bioorg. Med. Chem. 14 (2006) 3160–3173, https://doi.org/10.1016/j.bmc.2005.12.032.

[65] H. Sharma, N. Kaur, A. Singh, A. Kuwar, N. Singh, Optical chemosensor for water sample analysis, J. Mater. Chem. C 4 (2016) 5154–5194, https://doi.org/10.1039/C6TC00605A.

[66] P.G. Mahajan, N.C. Dige, B.D. Vanjare, H. Raza, M. Hassan, S.Y. Seo, C.H. Kim, K.H. Lee, Facile synthesis of new quinazolinone benzamides as potent tyrosinase inhibitors: comparative spectroscopic and molecular docking studies, J. Mol. Struct. 1198 (2019) 126915, https://doi.org/10.1016/j.molstruc.2019.126915.

[67] X.F. Zhang, J. Zhang, L. Liu, Fluorescence properties of twenty fluorescein derivatives: lifetime, quantum yield, absorption and emission spectra, J. Fluoresc. 24 (2014) 819–826, https://doi.org/10.1007/s10895-014-1356-5.

[68] M. Hassan, Q. Abbas, Z. Ashraf, A.A. Moustafa, S.Y. Seo, Pharmacoinformatic exploration of polyphenol oxidases leading to novel inhibitors by virtual screening and molecular dynamic simulation study, Comput. Biol. Chem. 68 (2017) 131–142, https://doi.org/10.1016/j.compbiolchem.2017.02.012.

[69] M. Hanif, F. Kanwal, M. Rafiq, M. Hassan, M. Mustaqeem, S.Y. Seo, Y. Zhang, C. Lu, T. Chen, M. Saleem, Symmetrical heterocyclic cage skeleton: synthesis, urease inhibition activity, kinetic mechanistic insight, and molecular docking analyses, Molecules 24 (2019) 312, https://doi.org/10.3390/molecules24020312.